Thermal Analysis
Information for Users

54
User Com

**Dear Customer,**

The steadily growing world population is faced with numerous problems such as the access to water, the supply of sufficient food for everyone and the unequal distribution of wealth. However, topics in the field of environmental protection and sustainable energy production are also rapidly gaining more and more attention.

In automotive engineering, it seems that the decision to end the production of petrol and diesel engines has already been taken. Numerous automobile manufacturers have already begun or at least planned a rapid change to electromobility. The environmentally friendly $CO_2$-free generation of electrical energy and its mobile storage remains a great challenge for most countries. Thermal analysis can make a valuable contribution to solving these problems, many of which are closely connected with materials research.

We hope you will find the articles in this latest issue of UserCom interesting and welcome your comments and feedback.

The METTLER TOLEDO thermal analysis team

# Isothermal calibration and adjustment, Part 2: Heating rate dependence of temperature measurement

Dr. Teresa Dennenwaldt, Jessica Stromer

**Adjustment or calibration at just one heating rate does not provide complete information about temperature accuracy. The temperature error has a dynamic and an isothermal component because it is not possible to position a temperature sensor inside the sample. In this article, we show how a thermal analysis instrument can be adjusted so that the temperature is independent of the heating rate. This is particularly important for isothermal measurements.**

## Contents 2/2021



METTLER TOLEDO

## Introduction

Correct adjustment (changing the adjustment parameters) and calibration (determination of deviation) of an instrument are essential for good measurements and accurate results. The calibration methods stored in the STARe software can be used for both adjustment and calibration. An instrument that has been adjusted and calibrated at only one heating rate should only be used at this heating rate. Correct tau lag adjustment is a key requirement for measuring precise temperatures both at different heating rates and isothermally [1, 2]. Correct adjustment and calibration are particularly important when measurement results depend strongly on temperature for example in measurements performed isothermally as is often the case in sorption and oxidation studies (oxidation induction time, OIT) and delamination experiments [3, 4, 5].

Table 1.
Melting points of indium, tin and lead.

| | $T_m$ in °C | Adjustment | Calibration |
|---|---|---|---|
| Indium | 156.6 | x | x |
| Tin | 231.9 | – | x |
| Lead | 327.5 | x | x |

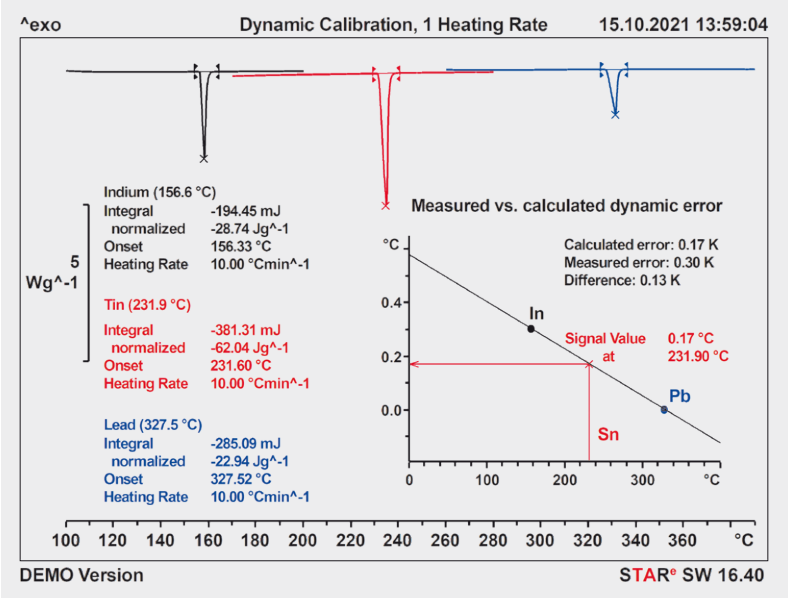


Figure 1.
Onset temperatures after temperature calibration using the Standard method (In, Sn and Pb, 10 K/min), as well as the measured and calculated temperature deviation at 231.9 °C (below right).

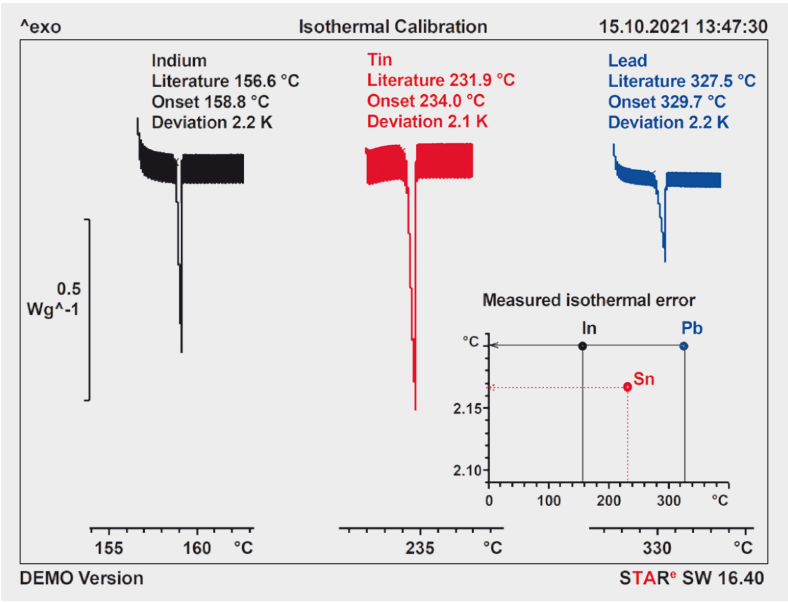


Figure 2.
Isothermal temperature calibration (In, Sn and Pb) using the isothermal Step method as well as the isothermal temperature deviation as a function of temperature (below right).

## Experimental details

The measurements were carried out using a DSC equipped with an intracooler and a sample robot. Three reference substances were used (Table 1).

The indium sample was prepared from a flat piece of indium. The weight of the sample should be 4 to 8 mg. The tin and lead samples were prepared similarly with sample weights of 4 to 8 mg for tin and 6 to 14 mg for lead. The samples were measured in 40-µL aluminum crucibles with aluminum lids that were pierced before sealing. A reactive gas was not used.

The TMA measurements were carried out using a TMA/SDTA equipped with an intracooler. The SDTA signal was measured using a flat piece of indium placed in a 40-µL aluminum crucible. The lid was pierced beforehand. The sample weight should be between 10 and 22 mg. The length signal was determined by placing a small piece of indium (about 0.5 mm thick) between two quartz disks and measuring the sample height.

The TGA measurements were carried out using a TGA/DSC. Samples were prepared in the same way as for the SDTA experiment in the TMA.

## Evaluation and results

The DSC was adjusted with indium and lead using the Calib DSC Standard method, which employs one single heating rate of 10 K/min, and then calibrated with indium, tin and lead. Isothermal calibration was performed using the isothermal Step method with 0.1 K steps and 30 s intervals for indium, tin and lead.

For comparison, the DSC was adjusted with indium and lead using the Calib DSC Expert method at three heating

rates of 2, 5 and 10 K/min and then calibrated with indium, tin and lead. This adjustment adjusts all three parameters (tau lag, temperature and enthalpy) in one single measurement. The isothermal calibration was carried out using the isothermal Step method with indium, tin and lead.

Isothermal calibration using the Isostep method was also performed for the TGA/DSC and the TMA/SDTA. The measurement of length change in the TMA was carried out using the Isostep method with 0.1 K steps, 1 min intervals and a force of 0.1 N. The sample support was a ball point probe (3 mm) made of quartz glass. The steps for the determination of the temperature change were increased to 0.2 K in the TMA/SDTA and TGA/DSC experiments. The results obtained are discussed in the following sections.

## Correct dynamic calibration of the DSC without isothermal calibration

The dynamically measured temperature can be perfectly correct for one single heating rate but wrong for all other heating rates and isothermal temperatures. Figure 1 shows the onset temperatures for indium, tin and lead for a heating rate of 10 K/min after temperature calibration using the Standard method. The DSC was adjusted with indium and lead and calibrated with indium (black), tin (red) and lead (blue). The purpose of the tin measurement was to check the temperature deviation at 231.9 °C (melting point of tin) after the Standard calibration (Figure 1, below right). The calculated value determined from the diagram at 231.9 °C (melting point of tin) was 0.17 K and the measured value 0.3 K. This gives a deviation of only 0.13 K. Dynamic measurements in this temperature range at a heating rate of 10 K/min yield correct temperature results. But what is the situation with isothermal measurements? Figure 2 shows an isothermal temperature calibration using the isothermal Step method with indium, tin and lead. Evaluation of the temperature

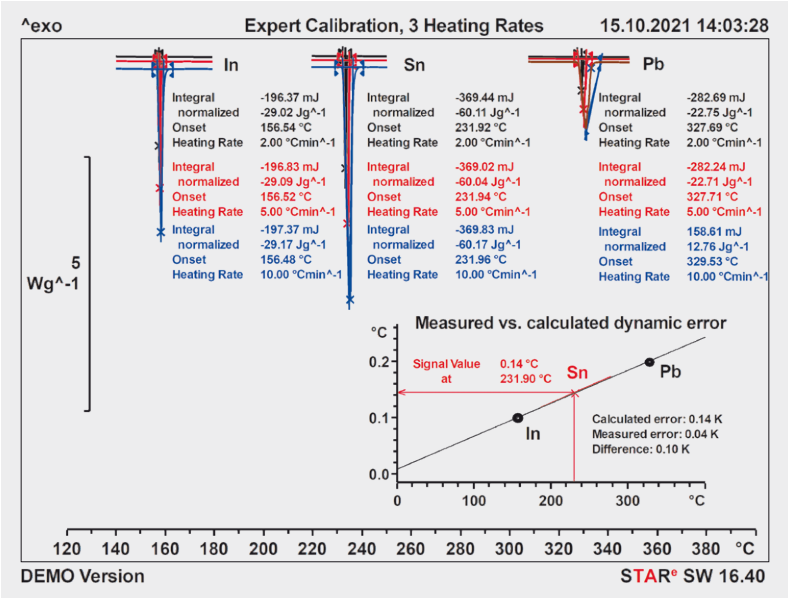


Figure 3.
Onset temperatures after Expert calibration (In, Sn and Pb) at heating rates of 2, 5 and 10 K/min as well as the measured temperature deviation at 231.9 °C after Expert calibration (below right).

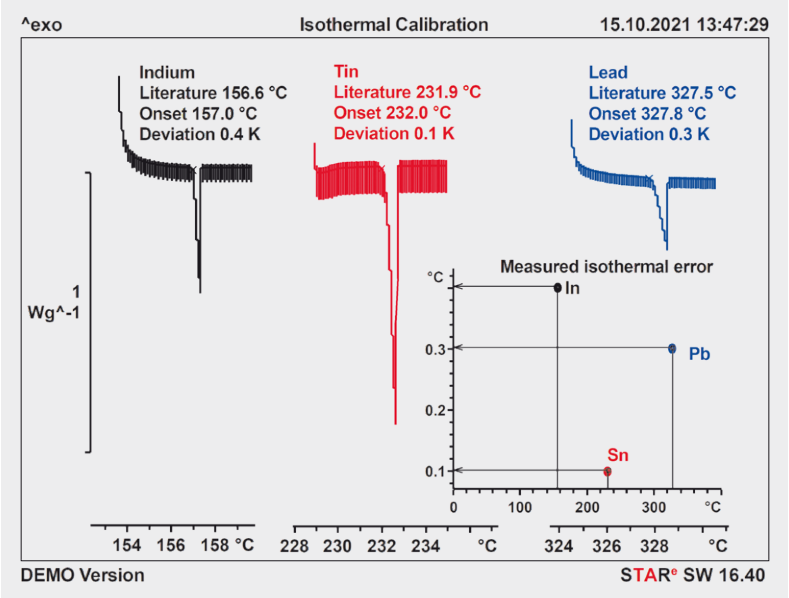


Figure 4.
Isothermal temperature calibration (In, Sn and Pb) using the isothermal Step method as well as the isothermal temperature deviation as a function of the temperature after tau lag adjustment (below right).

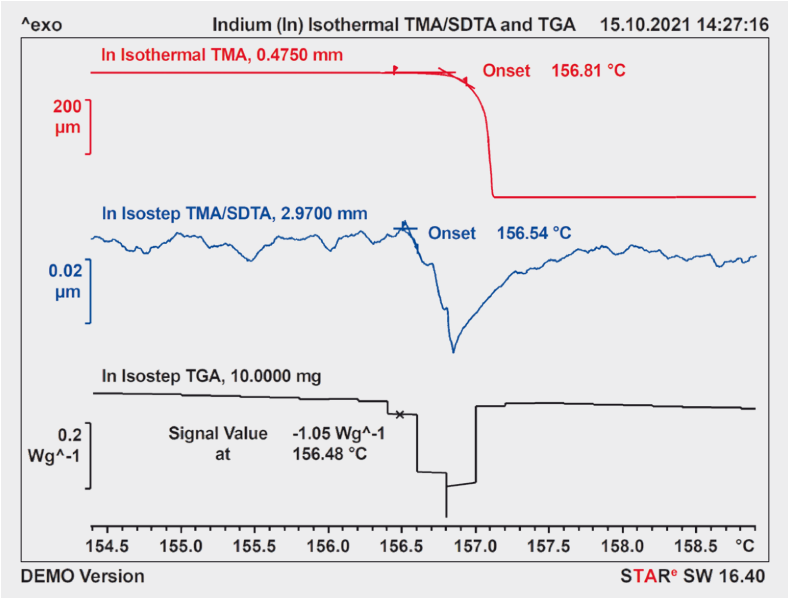


Figure 5.
Almost perfect temperature agreement of the isothermal Step method of the TMA signal (red), the TMA/SDTA signal (blue), and the TGA/DSC signal (black).

deviation (Figure 2, below right) yields isothermal deviations of 2.1 and 2.2 K. This means that if we performed an experiment isothermally, for example at 70 °C, the temperature deviation would be more than 2 K. This could lead to quite serious errors in the results of delamination, sorption or OIT measurements. The dynamically measured temperature can therefore be perfectly correctly adjusted and calibrated for a single heating rate but wrong for measurements for all other heating rates and isothermal temperatures.

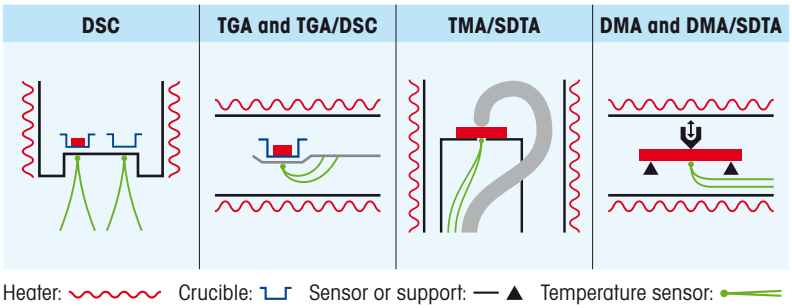


Figure 6.
Schematic diagram of the temperature sensors in thermal analysis instruments.

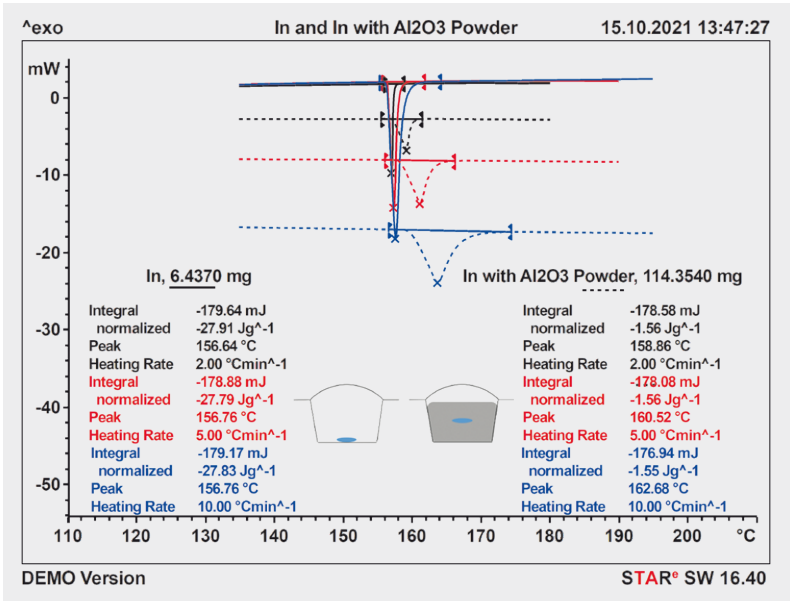


Figure 7.
DSC curves of indium in an aluminum crucible. The indium was placed on the bottom of the crucible (upper curves, solid lines) and embedded in aluminum oxide powder (lower curves, dashed lines).

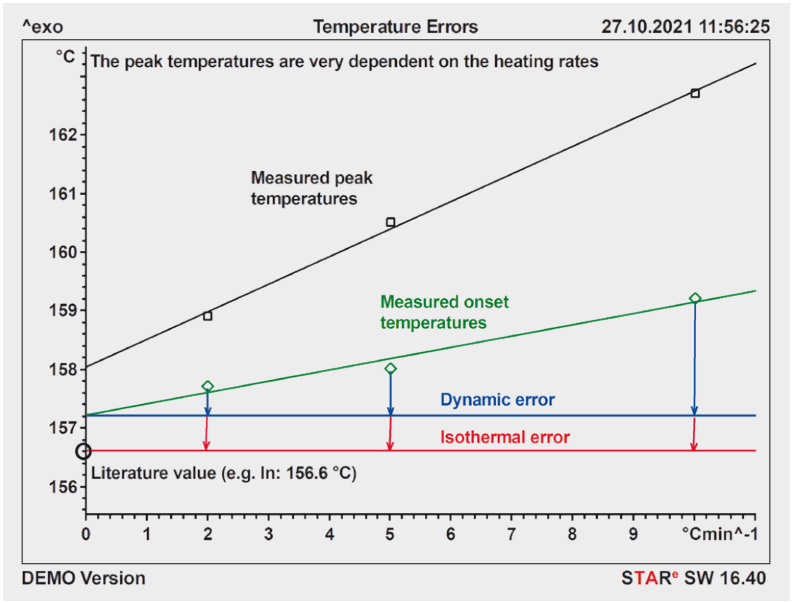


Figure 8.
Difference between the dynamic and the isothermal error. The slope of the line corresponds to tau lag, the time delay between the measurement point and the sample.

## Correct dynamic and isothermal calibration of the DSC

Figure 3 shows the onset temperatures of the DSC after it was calibrated using Expert adjustment with indium, tin and lead for heating rates of 2, 5 and 10 K/min. The calculated error is 0.14 K and the measured error 0.04 K. This gives a difference of only 0.1 K (Figure 3, below right). Evaluation of the isothermal Step method for indium, tin and lead (Figure 4) confirms that after correct Expert adjustment (tau lag adjustment) there is only a small temperature deviation of 0.1 to 0.4 K. This means that a maximum temperature deviation of 0.35 K would be expected for an experiment performed at 70 °C. Expert adjustment provides exact results both for dynamic and for isothermal temperature programs.

## Correct dynamic and isothermal calibration of the TGA and TMA

Both the TGA and the TMA can be adjusted in a similar way so that temperatures are independent of the heating rate (Expert adjustment method). This is followed by the calibration measurement. The isothermal Step method can be used for the TGA; the DSC signal is evaluated. The TMA can be adjusted and calibrated by means of two different isothermal Step methods:

1. Using the length change (limited to one single heating rate) and
2. Using the sample temperature (SDTA signal), suitable for Expert adjustment

The evaluations are shown in Figure 5. All three evaluation methods give the correct onset temperature for indium.

## Dynamic and isothermal temperature error

A temperature deviation is the result of two factors. First, the sensor itself may be faulty; this corresponds to the isothermal part. The other factor is that the sensor is not directly inside the sample being measured but lies outside the crucible; this gives rise to a dynamic error.

Two experiments were performed to illustrate this behavior (Figure 7).

**OIT (DSC)**

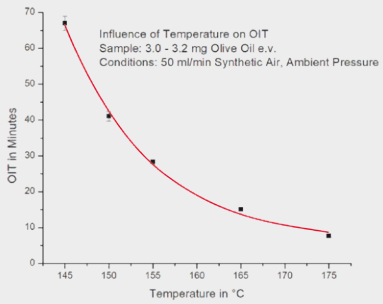


Dependence of oxidation on the temperature.

**Sorption (TGA, TMA and DMA)**

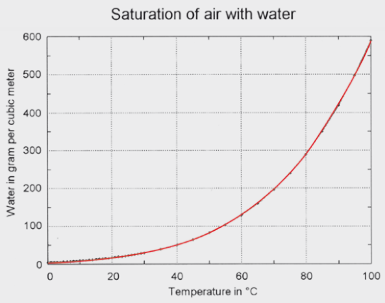


Saturation curve of air with water at different temperatures.

**Delamination (TMA)**

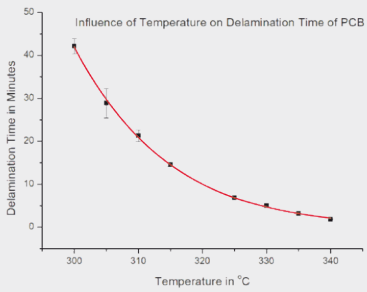


Delamination times of PCB at different temperatures.

Figure 9.
These applications exhibit strong non-linear temperature dependence.

An indium pill was placed directly on the bottom of an aluminum crucible and heated at three different heating rates in a correctly adjusted and calibrated DSC. This experimental setup simulates the situation in which the sensor is inside the sample. Within the tolerance limits, the onset temperatures lie close to the literature value. However, if the indium pill is embedded in inert aluminum oxide powder, the sample volume and mass are greatly increased. This has a marked effect on the heat flow signal [6]. It leads to a large start-up signal due to the larger heat capacity of the entire sample. The poorer thermal conductivity of the aluminum oxide powder slows down the heat flow to the indium and causes the onset temperature to shift to higher temperature (see Table 2).

| Heating rate in K/min | Onset temperature in °C (indium placed on the bottom of the crucible) | Onset temperature in °C (indium embedded in aluminum oxide powder) |
|---|---|---|
| 2 | 156.4 | 157.1 |
| 5 | 156.4 | 158 |
| 10 | 156.3 | 159.2 |

Table 2.
Measured onset temperatures of indium on the crucible bottom (middle column) and embedded in alumina powder (right column).

This experimental setup simulates the extreme case in which the sensor lies outside the sample. The onset temperatures no longer correspond to the literature value and deviate more and more from this at increasing heating rates. The experiment is shown graphically in Figure 8.

## Conclusions

The accuracy of the isothermal temperature has a very large influence on the result in the applications in Figure 9.

The examples show how strongly oxidation, sorption and delamination depend on temperature. The higher the temperature, the faster the reaction proceeds (Figure 9). The trend is exponential. We will cover this in more detail in future UserCom articles of this series.

## Summary

In this article, different adjustment and calibration methods for the DSC, TGA and TMA have been presented and compared with one another, in particular with regard to isothermal measurements. Different reference substances are suitable for adjustment and calibration, depending on the temperature range involved [1, 7, 8].

After dynamic calibration of an instrument using the Standard method at one single heating rate, the calculated and the measured errors of a reference substance are in good agreement with literature values. However, the calibration for other heating rates or the special case of isothermal temperature can be quite different.

After Expert calibration, which involves the use of different heating rates, both the dynamic and the isothermal calibration measurements are in almost perfect agreement with the reference temperatures. Expert adjustment requires a calibration method using at least three different heating rates. Heating rate independence cannot therefore be achieved using standard methods at one single heating rate. The Expert method or the isothermal Step method can be useful to check whether onset temperatures change at different heating rates. If this is the case, adjustment must be repeated.

## References


[1] Calibration, UserCom 6, 1–5.
[2] Matthias Wagner, METTLER TOLEDO Collected Applications Handbook, Thermal Analysis in Practice.
[3] Marco Zappa, Influence of absorbed moisture on the mechanical properties of Polyamide, UserCom 24, 1–5.
[4] Jacques Besse, Mathieu Zongo, Stability studies of fish oils by high-pressure DSC, UserCom 32, 9–11.
[5] Cyril Darribère, Investigation of delamination and foaming by TMA-MS, UserCom 15, 21–22.
[6] Kai Hassdenteufel, Influence of the sample volume in the high-pressure on the DSC signal, to be published.
[7] Markus Schubnell, Domenico Regonini, Calibration and adjustment of DSCs, Part 1: Which materials are suitable? UserCom 53, 1– 6.
[8] Ben Joseph, Certified reference materials for thermal analysis from LGC, UserCom 24, 9–10.


**For more information:**
**www.mt.com/ta-calibration**

# New reference library versions

Our "Reference Library" option is very popular and in great demand. Users value its enormous flexibility, in particular with regard to the following features:

1. the number of result columns,
2. the addition of a user's own information such as text, other physical values, entire documents, images or videos,
3. the combination of different measurement techniques and
4. the different search possibilities.

Figure 1.
Section of the PCM reference library.

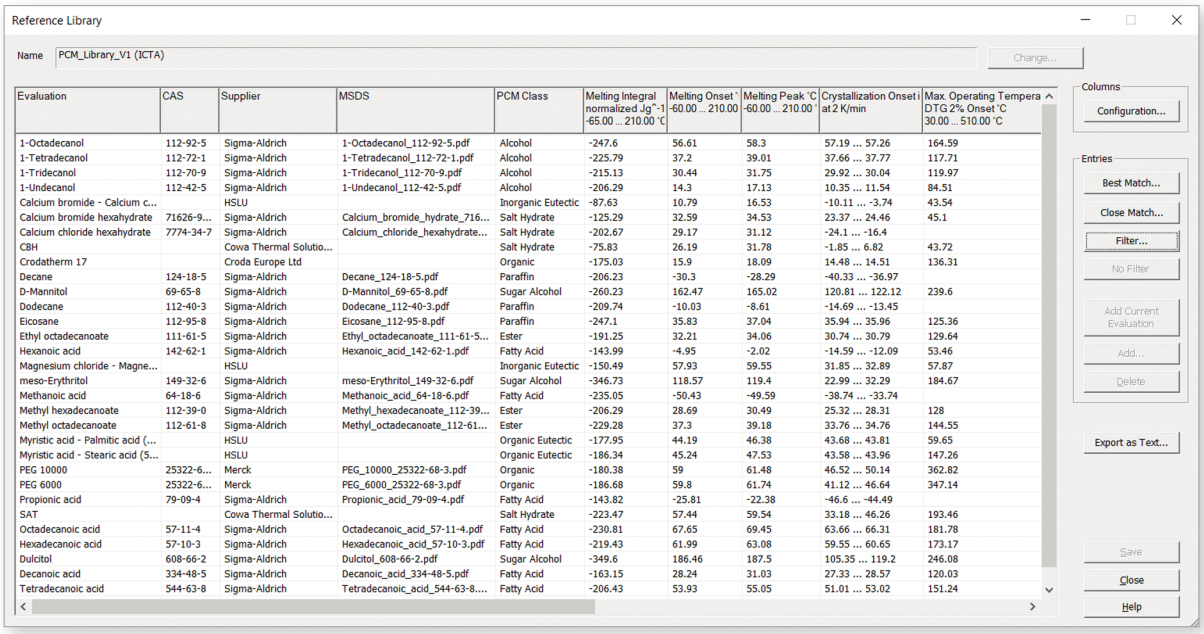


| Evaluation | CAS | Supplier | MSDS | PCM Class | Melting Integral normalized Jg⁻¹ -65.00 ... 210.00 °C | Melting Onset ° -60.00 ... 210.00 | Melting Peak °C -60.00 ... 210.00 | Crystallization Onset i at 2 K/min | Max. Operating Tempera DTG 2% Onset °C 30.00 ... 510.00 °C |
|---|---|---|---|---|---|---|---|---|---|
| 1-Octadecanol | 112-92-5 | Sigma-Aldrich | 1-Octadecanol_112-92-5.pdf | Alcohol | -247.6 | 56.61 | 58.3 | 57.19 ... 57.26 | 164.59 |
| 1-Tetradecanol | 112-72-1 | Sigma-Aldrich | 1-Tetradecanol_112-72-1.pdf | Alcohol | -225.79 | 37.2 | 39.01 | 37.66 ... 37.77 | 117.71 |
| 1-Tridecanol | 112-70-9 | Sigma-Aldrich | 1-Tridecanol_112-70-9.pdf | Alcohol | -215.13 | 30.44 | 31.75 | 29.92 ... 30.04 | 119.97 |
| 1-Undecanol | 112-42-5 | Sigma-Aldrich | 1-Undecanol_112-42-5.pdf | Alcohol | -206.29 | 14.3 | 17.13 | 10.35 ... 11.54 | 84.51 |
| Calcium bromide - Calcium c... | | HSLU | | Inorganic Eutectic | -87.63 | 10.79 | 16.53 | -10.11 ... -3.74 | 43.54 |
| Calcium bromide hexahydrate | 71626-9... | Sigma-Aldrich | Calcium_bromide_hydrate_716... | Salt Hydrate | -125.29 | 32.59 | 34.53 | 23.37 ... 24.46 | 45.1 |
| Calcium chloride hexahydrate | 7774-34-7 | Sigma-Aldrich | Calcium_chloride_hexahydrate... | Salt Hydrate | -202.67 | 29.17 | 31.12 | -24.1 ... -16.4 | |
| CBH | | Cowa Thermal Solutio... | | Salt Hydrate | -75.83 | 26.19 | 31.78 | -1.85 ... 6.82 | 43.72 |
| Crodatherm 17 | | Croda Europe Ltd | | Organic | -175.03 | 15.9 | 18.09 | 14.48 ... 14.51 | 136.31 |
| Decane | 124-18-5 | Sigma-Aldrich | Decane_124-18-5.pdf | Paraffin | -206.23 | -30.3 | -28.29 | -40.33 ... -36.97 | |
| D-Mannitol | 69-65-8 | Sigma-Aldrich | D-Mannitol_69-65-8.pdf | Sugar Alcohol | -260.23 | 162.47 | 165.02 | 120.81 ... 122.12 | 239.6 |
| Dodecane | 112-40-3 | Sigma-Aldrich | Dodecane_112-40-3.pdf | Paraffin | -209.74 | -10.03 | -8.61 | -14.69 ... -13.45 | |
| Eicosane | 112-95-8 | Sigma-Aldrich | Eicosane_112-95-8.pdf | Paraffin | -247.1 | 35.83 | 37.04 | 35.94 ... 35.96 | 125.36 |
| Ethyl octadecanoate | 111-61-5 | Sigma-Aldrich | Ethyl_octadecanoate_111-61-5... | Ester | -191.25 | 32.21 | 34.06 | 30.74 ... 30.79 | 129.64 |
| Hexanoic acid | 142-62-1 | Sigma-Aldrich | Hexanoic_acid_142-62-1.pdf | Fatty Acid | -143.99 | -4.95 | -2.02 | -14.59 ... -12.09 | 53.46 |
| Magnesium chloride - Magne... | | HSLU | | Inorganic Eutectic | -150.49 | 57.93 | 59.55 | 31.85 ... 32.89 | 57.87 |
| meso-Erythritol | 149-32-6 | Sigma-Aldrich | meso-Erythritol_149-32-6.pdf | Sugar Alcohol | -346.73 | 118.57 | 119.4 | 22.99 ... 32.29 | 184.67 |
| Methanoic acid | 64-18-6 | Sigma-Aldrich | Methanoic_acid_64-18-6.pdf | Fatty Acid | -235.05 | -50.43 | -49.59 | -38.74 ... -33.74 | |
| Methyl hexadecanoate | 112-39-0 | Sigma-Aldrich | Methyl_hexadecanoate_112-39... | Ester | -206.29 | 28.69 | 30.49 | 25.32 ... 28.31 | 128 |
| Methyl octadecanoate | 112-61-8 | Sigma-Aldrich | Methyl_octadecanoate_112-61... | Ester | -229.28 | 37.3 | 39.18 | 33.76 ... 34.76 | 144.55 |
| Myristic acid - Palmitic acid (... | | HSLU | | Organic Eutectic | -177.95 | 44.19 | 46.38 | 43.68 ... 43.81 | 59.65 |
| Myristic acid - Stearic acid (5... | | HSLU | | Organic Eutectic | -186.34 | 45.24 | 47.53 | 43.58 ... 43.96 | 147.26 |
| PEG 10000 | 25322-6... | Merck | PEG_10000_25322-68-3.pdf | Organic | -180.38 | 59 | 61.48 | 46.52 ... 50.14 | 362.82 |
| PEG 6000 | 25322-6... | Merck | PEG_6000_25322-68-3.pdf | Organic | -186.68 | 59.8 | 61.74 | 41.12 ... 46.64 | 347.14 |
| Propionic acid | 79-09-4 | Sigma-Aldrich | Propionic_acid_79-09-4.pdf | Fatty Acid | -143.82 | -25.81 | -22.38 | -46.6 ... -44.49 | |
| SAT | | Cowa Thermal Solutio... | | Salt Hydrate | -223.47 | 57.44 | 59.54 | 33.18 ... 46.26 | 193.46 |
| Octadecanoic acid | 57-11-4 | Sigma-Aldrich | Octadecanoic_acid_57-11-4.pdf | Fatty Acid | -230.81 | 67.65 | 69.45 | 63.66 ... 66.31 | 181.78 |
| Hexadecanoic acid | 57-10-3 | Sigma-Aldrich | Hexadecanoic_acid_57-10-3.pdf | Fatty Acid | -219.43 | 61.99 | 63.08 | 59.55 ... 60.65 | 173.17 |
| Dulcitol | 608-66-2 | Sigma-Aldrich | Dulcitol_608-66-2.pdf | Sugar Alcohol | -349.6 | 186.46 | 187.5 | 105.35 ... 119.2 | 246.08 |
| Decanoic acid | 334-48-5 | Sigma-Aldrich | Decanoic_acid_334-48-5.pdf | Fatty Acid | -163.15 | 28.24 | 31.03 | 27.33 ... 28.57 | 120.03 |
| Tetradecanoic acid | 544-63-8 | Sigma-Aldrich | Tetradecanoic_acid_544-63-8.... | Fatty Acid | -206.43 | 53.93 | 55.05 | 51.01 ... 53.02 | 151.24 |

The freely available material libraries are being constantly expanded and can be used as the basis for building your own library. The current libraries can be downloaded at www.mt.com/ta-libraries. The following new libraries are available, the number of different materials is given in brackets:

- Elastomers V3 (43 → 57 examples)
- Pharmaceuticals V3 (43 → 70 examples)
- New: Inorganics V1 (24 examples)

# The new Validation in Thermal Analysis handbook

We are delighted to announce the revised edition of the Validation in Thermal Analysis handbook. The first edition was published in 2008. In the new handbook, Part 1 "Validation of computerized systems" has been completely revised and Part 2 "Method Validation" has been corrected where necessary and otherwise brought completely up to date. Validation is in fact even more relevant today than it was 13 years ago. Ensuring the quality of results is equally important as data integrity and data security.

The book is intended for users of thermal analysis who want to improve the quality of their results by method validation. Three possible approaches are available:

1. the use of a standard (ISO, DIN, ASTM, etc.),
2. the use of a method that has been "validated" by means of round-robin tests or
3. analytical method validation.

Further valuable information on this can be found in the new handbook under www.mt.com/ta-handbooks.

# User manuals and other useful aids

There is often not enough time to read a user manual before putting a system into operation. Nevertheless, it is useful to know where the manual is if it is needed. We are aware that there are many ways to become an expert. You can find lots of information in our different manuals, for example on how to get better results or prevent damage to instruments and risks to personal.

In addition to the product manuals, we also offer other aids that can help you become an expert.

| | STAR$^{e}$ software | Instruments |
|---|---|---|
| Online Help | X, with integrated videos | – |
| User Manual | X | X |
| Reference Manual | X | X |
| Operating Instructions | – | X |
| Services that were presented in UserCom 53 | www.mt.com/ta-services | |

Although all the relevant documents are supplied together with the system purchased, they can't always be found in a hurry. At www.mt.com/ta-manuals you can quickly find the manuals you need for your STAR$^{e}$ software version or your instrument. You can download the relevant documentation for the current product or for products that are no longer in our sales program.

On the same page in the Internet, you will also find:

1. Current STAR$^{e}$ Software Patches,
2. Free Evaluation Software (license-free Evaluation Window),
3. STAR$^{e}$ Software Language Packs (English, German, French, Russian, Korean, Chinese and Japanese),
4. Instrument Software Updates.

We hope that our comprehensive documentation will enable you to quickly solve your problems by thermal analysis and achieve the best possible results.

# Characterization of gelatin and gelatin gels by TGA/DSC-MS, DSC and TMA

Dr. Markus Schubnell

**Gelatin is an important basic raw material for the food and pharmaceutical industries. For example, in the food industry, gelatin is used as a gelling agent in confectionery, and in the pharmaceutical industry for the manufacture of capsules containing active ingredients. In this article, we show how gelatin and gelatin gels can be characterized by TGA/DSC-MS, DSC and TMA.**

## Introduction

Gelatin is widely used in the food industry, for example as a gelling agent in confectionery (jelly bears), for jellied meat products (aspic jellies) or for bakery products (glazing), and in the pharmaceutical industry to make hard and soft capsules for drug products and as a thickening agent for liquid pharmaceuticals.

Gelatin consists of partially hydrolyzed collagen, which is mainly extracted from the bones, skins and tissues of cattle, pigs and poultry. It is therefore not a pure chemical product but consists of amino acids that are linked together with peptide bonds to long chain proteins with molecular weights between 15,000 and 400,000 g/mol. Gelatin swells when immersed in cold water. If the swollen gelatin is heated, a colloidal solution (a sol) is formed. This destroys the original structure of the gelatin-protein (denaturation). On cooling, the solution forms a three-dimensional network in which the original structure of the gelatin-protein is restored (renaturation) and the water remains integrated in the network. This results in a rubbery-like gel. This process is reversible, which is why the gelatin gels are also known as thermoreversible gels.

In this article, we show how gelatins and gelatin gels can be investigated using different thermal analysis methods (TGA/DSC-MS, DSC, TMA).

## Experimental details

The sample investigated was a gelatin powder obtained from a local supermarket. The gelatin was first characterized by TGA/DSC coupled to a mass spectrometer and by DSC (details follow later).

The gelatin gels were measured using gels with gelatin contents of 5%, 7.5%, 10%, 15% and 20%. The gels were prepared in sealable glass cells by mixing 300 mg gelatin and the appropriate volume of cold water needed to give the desired concentration. After a swelling time of 10 minutes, the (sealed) glass cell was heated in a water bath to 50 °C. The cell was left in the water bath with gentle shaking until the gelatin had completely dissolved in the water (no schlieren effects visible). The gelatin/water solution was then kept at 5 °C for 3 hours. Typically, 50 mg of each gelatin gel prepared in this way was then weighed into a hermetically sealed 100-µL aluminum crucible and measured in a DSC 3+ equipped with an intracooler and an FRS 6+ sensor. The temperature program consisted of cooling from room temperature to –5 °C at 5 K/min, followed by a heating-cooling-heating cycle between –5 °C and 50 °C at 5 K/min. In each case, the second heating run was evaluated.

Isothermal experiments were also carried out at different temperatures in order to investigate gel formation as a function of time and temperature (see DSC measurements of gelatin gels).

The TMA measurements were performed with a TMA/SDTA 2+ equipped with a 3-mm flat probe using gel samples that had been prepared for

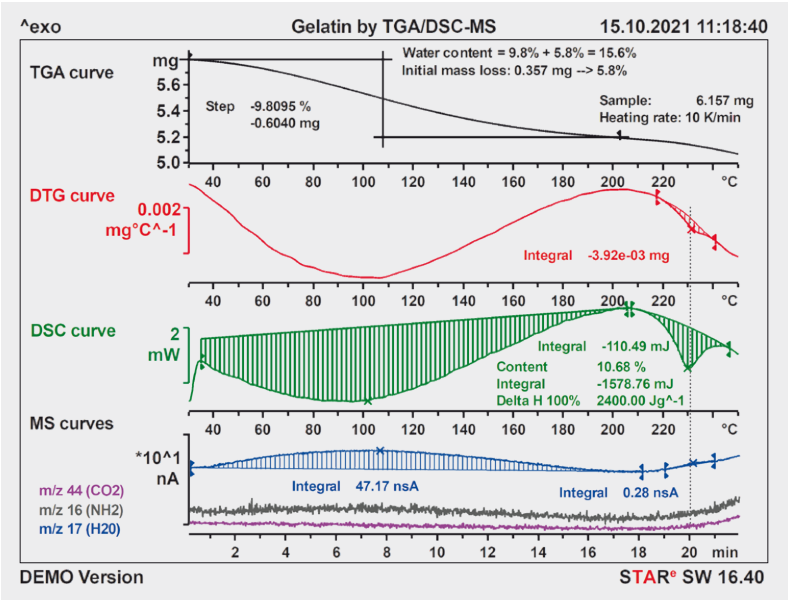


Figure 1. Determination of the water content of the gelatin by TGA/DSC and mass spectrometry (MS). The heating rate was 10 K/min.

the DSC measurements. About 50 mg of the gel sample was put into a hermetically sealed 100-µL aluminum crucible, heated to 50 °C in the TMA and then cooled to room temperature (cooling rate 5 K/min). The lid of the crucible was then removed and the sample cooled to –5 °C (cooling rate 5 K/min, applied force –0.1 N, that is, the probe was not in contact with the sample). The sample was then heated from –5 °C to 50 °C at a heating rate 5 K/min (force: sinusoidal DLTMA, force range between 0.02 N and 0.05 N). This procedure ensured that the samples measured had the same thermal history as the samples measured by DSC. In addition, the isothermal formation of a gelatin gel with a content of 10% gelatin was measured at 7.5 °C (see Gel formation, sol to gel).

## Results

### Characterization of the gelatin used

#### TGA/DSC-MS measurements

The gelatin used was characterized by TGA/DSC mass spectrometric analysis of the "dry" gelatin powder from the supermarket packet (heating rate 10 K/min, flow rate 50 mL/min nitrogen). The measurement curves obtained are shown in Figure 1. The TGA curve (black) and the corresponding DTG curve (first derivative of the TGA curve, red) show that the gelatin already begins to lose mass at the start of the measurement. One can see that two mass loss processes overlap. The DTG curve also indicates a further mass loss process that occurs at about 230 °C. Besides this, the sample mass at the beginning of the measurement was clearly less than the starting mass that was weighed in. The reason for this is that the sample was held at the start temperature for 15 minutes after it was inserted. This ensured that no oxygen or moisture was present in the furnace chamber when the sample was heated. During this time, the sample lost part of its original moisture content (5.8%). The rest of the moisture was released on heating (0.605 mg or 9.8%). The total water content was therefore about 15.6%.

The TGA/DSC curve (green) first shows a broad endothermic peak. The corresponding water content can be estimated from its area and the enthalpy of vaporization of water (assumption: 2400 J/g). The value obtained (11%) is comparable to the mass loss measured by TGA (10%). As observed in the DTG curve, the DSC curve also shows an endothermic peak at about 230 °C. The MS fragment ion curve of m/z 17 (water) identifies water both as moisture (between 30 and 210 °C) and as a decomposition product (from 210 °C onward). The increase of the MS ion curves for m/z 16 ($NH_2$) and m/z 44 ($CO_2$) confirm that decomposition begins from about 210 °C onward.

The small peak that appears at about 230 °C on the DTG and TGA/DSC curves is also observed on the MS ion curve for m/z 17. This therefore also seems to be due to water. Comparison of the ratio of the areas of the moisture peaks between 30 and 210 °C and around 230 °C calculated from the m/z 17 curve (47.2 nsA/0.28 nsA) or from the TGA and the DTG curves (0.6 mg/0.004 mg) yields values of

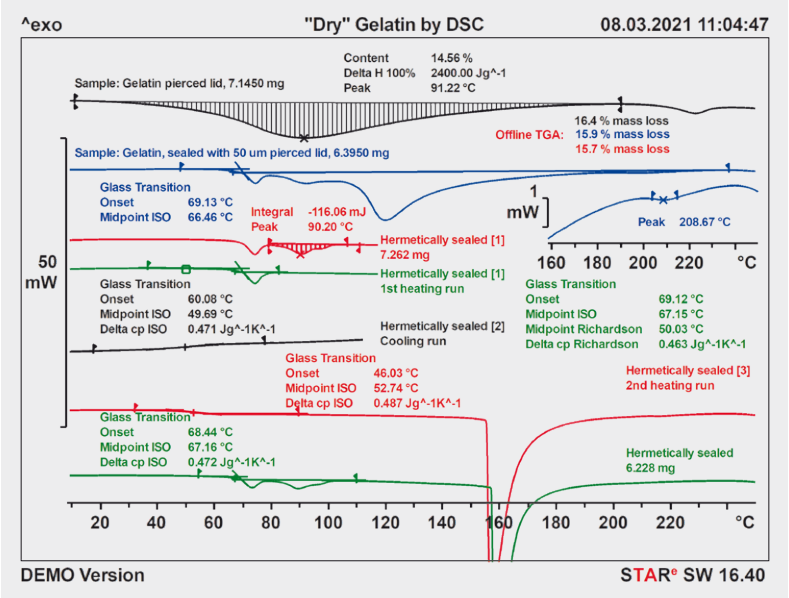


Figure 2.
DSC measurements of "dry" gelatin in open and hermetically sealed crucibles and in a crucible sealed with a 50-µm pierced lid. The heating and cooling rates were 10 K/min.

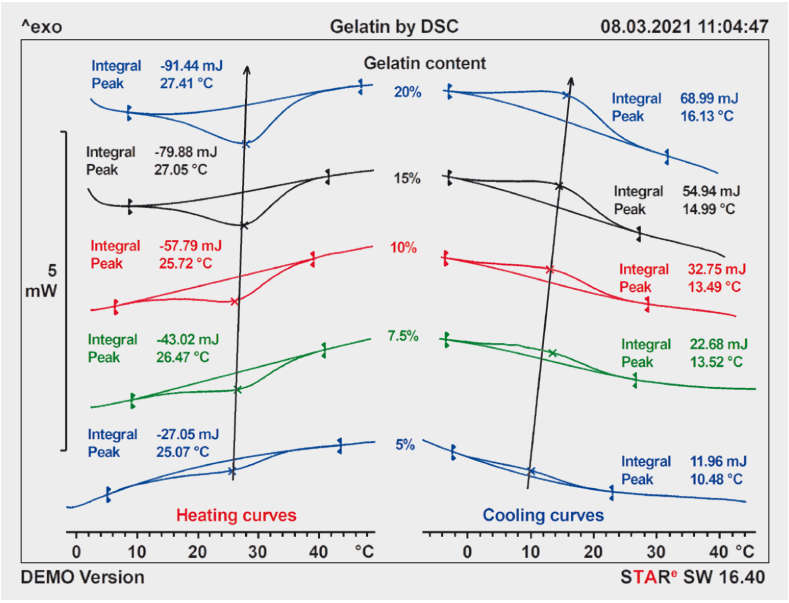


Figure 3.
Heating and cooling curves of gelatin gels with different gelatin contents.

168 and 150. Calculation of the same ratio from the TGA/DSC curve (1580 mJ /110 mJ) yields a value of 15. The difference of a factor of 10 between the ratios calculated from the TGA/DTG and the MS curve for m/z 17 and the corresponding value from the TGA/DSC curve cannot however be explained by the (large) uncertainty of the calculated ratios. This leads one to conclude that the small peak on the TGA/DSC curve not only contains the vaporization of about 4 µg water but also a significant contribution from another endothermic process. Additional DSC measurements were therefore performed in different sealed crucibles in order to understand this better.

## DSC measurements

The results of the DSC measurements are summarized in Figure 2. The experiments were carried out using different crucible setups:

- The black curve corresponds to the measurement of gelatin in a quasi-open crucible (large hole in the crucible lid).
- The blue curve was measured using a crucible sealed with a lid pierced with a 50-µm hole.
- The remaining curves were recorded using hermetically sealed crucibles. Here, one measurement was performed in three segments (heating to 120 °C, cooling to 5 °C, heating to 250 °C), and another measurement in one segment (5 to 250 °C, green curve, first heating run).

The red (1), green (1), black (2) and red (3) curves are different segments from one measurement. The green (1) curve is identical with the red (1) curve, except that the broad peak around 90 °C was replaced by a combination of a horizontal and a Spline-baseline (reason: this is the only way to evaluate the glass transition according to the Richardson method).

The heating and cooling rates were 10 K/min. In the quasi-open crucible (black curve), the DSC curve, just like the TGA/DSC curve, first shows a broad endothermic peak that characterizes the vaporization of water from the gelatin. As already observed in the TGA/DSC measurement, a second small endothermic peak follows at about 230 °C. If the crucible is sealed with a lid pierced with a 50-µm hole (blue curve), the vaporization process moves to higher temperatures. At 66 °C, a baseline shift occurs that can be interpreted as a glass transition. This is followed by two small endothermic peaks at about 72 °C and 92 °C. Besides this, there is a further small peak at 208 °C (see inset diagram).

If the sample is measured in a hermetically sealed crucible, the escape of moisture is completely suppressed. However, the pressure in the crucible increases with increasing temperature. This leads to the crucible bursting and the moisture suddenly escaping from the crucible. In the case of gelatin, this occurs at about 155 °C as shown by the large peaks in the green and red curves. The green curve shows a glass transition and the two peaks previously observed on the blue curve. In the final experiment, the first heating run using a hermetically sealed crucible was terminated at 120 °C. The DSC curve (red) is identical in this temperature range with the corresponding temperature range of the blue DSC curve (pierced lid) and the green curve (heating in a

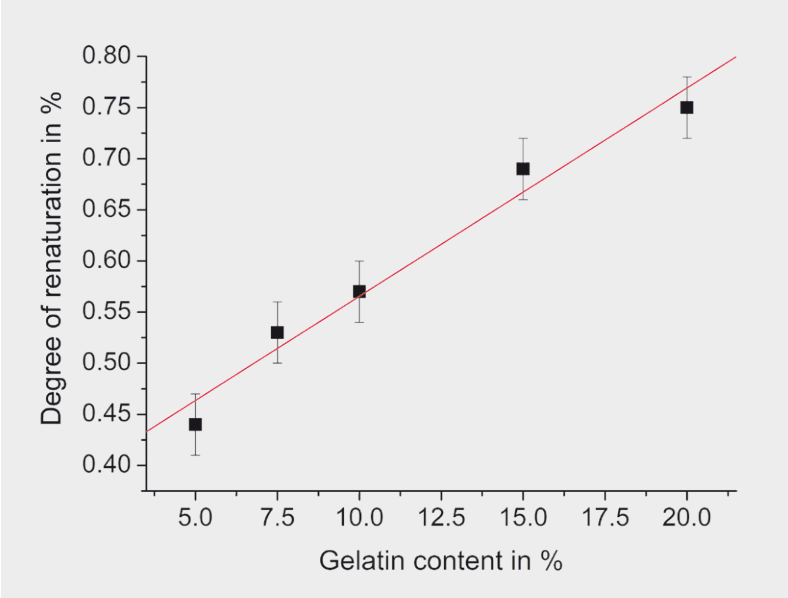


Figure 4.
Degree of renaturation of gels with different gelatin contents after cooling at 5 K/min from 50 °C to –5 °C.

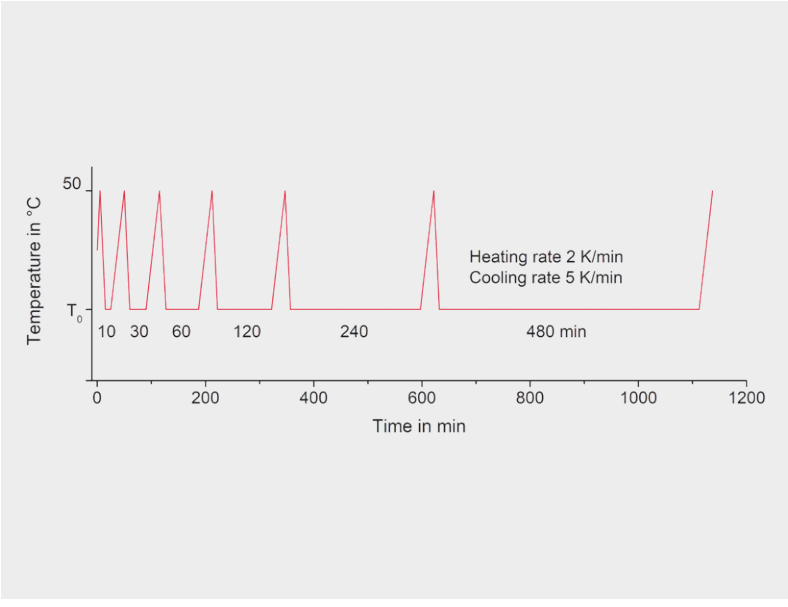


Figure 5.
Temperature program used to investigate the kinetics of the renaturation of gelatin gels; $T_0$ is the aging temperature.

hermetically sealed crucible). On cooling (black curve), the glass transition can be clearly seen at about 50 °C. This temperature is significantly lower than the $T_g$ midpoint observed during the first heating run. If the first peak at about 72 °C is interpreted as enthalpy relaxation, the glass transition can be evaluated according to the Richardson method. This procedure is used when one is interested in the $T_g$ of the material without enthalpy relaxation. The $T_g$ determined in this way should then agree with the $T_g$ determined on cooling or in a second heating run. This evaluation method can only be applied when the peak at 90 °C (which is not part of the enthalpy relaxation) is replaced by a suitable baseline. Technically this can be done using the STARe TA → Baseline function. The corrected DSC curve is shown in green. The $T_g$ evaluated using the Richardson method agrees well with $T_g$ values measured in the cooling run and the second heating run (about 50 °C). This means that the peak measured in the first heating run at 72 °C is in fact an enthalpy relaxation peak. This is also supported by the fact that the peak is no longer observed in the second heating run.

The peak that can be seen at about 90 °C in the curves measured with the hermetically sealed crucible and with the crucible sealed with a 50-µm pierced lid is due to the denaturation of the gelatin (at this temperature and under these conditions the gelatin still contains about 15% water). In an open crucible, denaturation occurs mainly at about 230 °C (at this temperature the gelatin is practically dry, see Figure 1). The TGA/DSC-MS measurement showed that a little water is also released as a result of the start of decomposition.

We interpret the small endothermic peak mentioned earlier at 208 °C on the DSC curve of the sample measured in an aluminum crucible sealed with a 50-µm pierced lid as the beginning decomposition of the completely denatured gelatin (blue curve in the inset diagram in Figure 2).

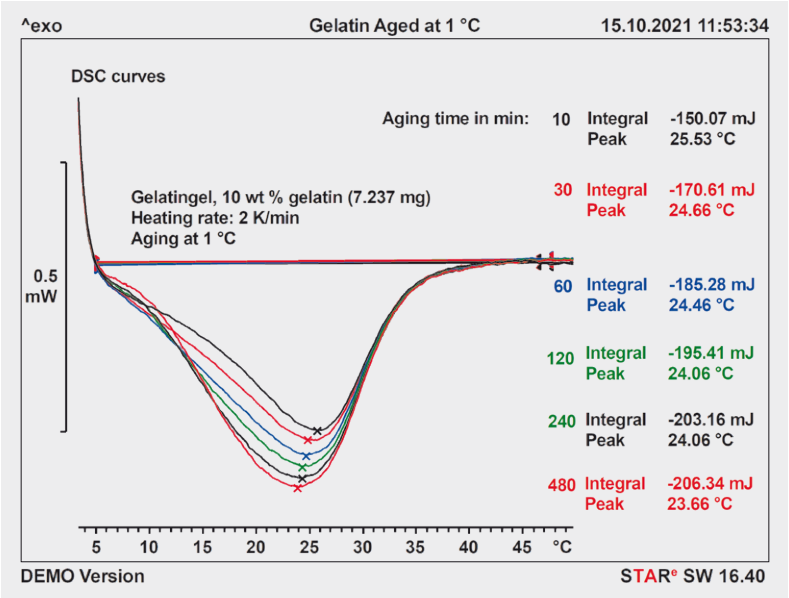


Figure 6. Denaturation peaks of a gelatin gel with 10 wt % gelatin held at 1 °C for different times (aging times).

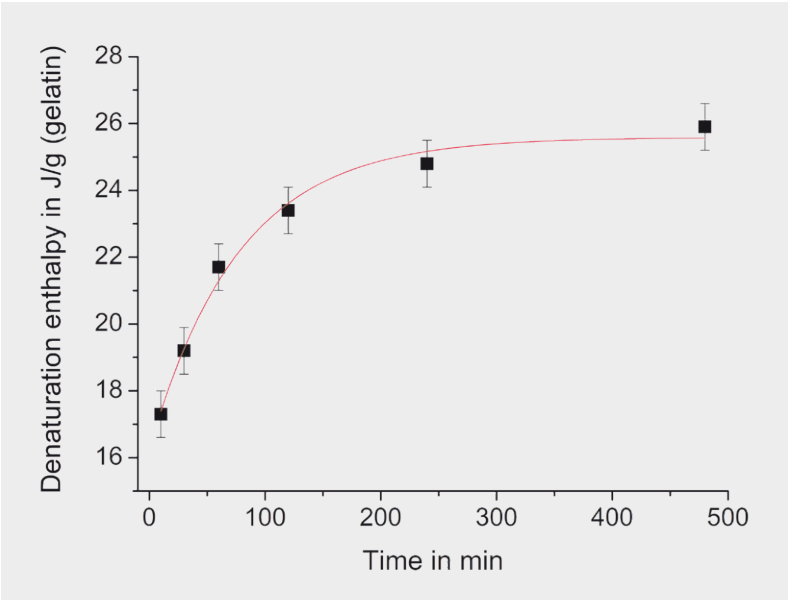


Figure 7. Curve showing denaturation enthalpy as a function of aging time using equation (1). The gelatin content of the gel was 10%.

## DSC measurements of gelatin gels

The sol or gel formation (denaturation and renaturation) of gelatin gels was investigated by measuring the gelatin gels described earlier (see Experimental details). Figure 3 shows the DSC curves of the gelatin gels with different gelatin contents; the second heating runs are shown on the left and the cooling runs on the right. The baselines for enthalpy determination are rather difficult to set. The measured enthalpies are therefore subject to a relatively large degree of uncertainty.

If the peak areas shown for the heating curves in Figure 3 are normalized to dry gelatin, a value of about 12.2 ± 1.2 J/(g gelatin) is obtained for the enthalpy of denaturation. The heating curves also show that the peak temperature of the denaturation peak is almost independent of the gelatin content, which is clearly not the case for renaturation. The renaturation enthalpies for the cooling rates of 5 K/min used here are also significantly smaller than the denaturation enthalpies. This means that during heating, renaturation continues to occur and presumably

also overlaps with denaturation (just as the crystallization and melting of polymers can overlap). The ratio of the renaturation enthalpy measured during cooling and the denaturation enthalpy measured during heating can be interpreted as a measure of the "degree of renaturation" after cooling at 5 K/min to –5 °C before heating. This is plotted in Figure 4 as a function of the gelatin content of the gel. The conclusion is that gel formation during cooling takes place more rapidly with high gelatin contents than with low gelatin contents.

It is unclear whether renaturation has occurred completely. Gelatin gels were therefore measured using the temperature program shown in Figure 5 in order to gain a better understanding of the kinetics of the renaturation. Here $T_0$ is the temperature at which the gel formation was investigated.

As an example, Figure 6 shows the DSC heating curves of a gelatin gel with a gelatin content of 10 wt % that was held at 1 °C for different times (aging times).

Figure 7 shows a plot of the denaturation enthalpy as a function of aging time using the values from Figure 6. The data shown in Figure 7 can be described using an exponential function (solid line curve) according to the equation:

$$\Delta H_{\text{denat}}(t) = \Delta H_{\text{denat}}^{\max} - \Delta H_{\text{denat}}^{i} \cdot \exp\left(-\frac{t}{\tau}\right) \quad (1)$$

Here $\Delta H_{\text{denat}}(t)$ is the denaturation enthalpy after an aging time $t$, $\Delta H_{\text{denat}}^{\max}$ the denaturation enthalpy of the completely renatured gel, $\Delta H_{\text{denat}}^{i}$ the contribution to the measured denaturation enthalpy which occurs after cooling (renaturation enthalpy during cooling = $\Delta H_{\text{denat}}^{\max} - \Delta H_{\text{denat}}^{i}$) and $\tau$ the time constant that characterizes the renaturation under isothermal conditions.

The data shown in Figure 7 yields a value of 77 minutes for $\tau$, the uncertainty (standard deviation) of 19 minutes is relatively large. This means that a 10% gelatin gel held at 1 °C reaches its maximum degree of formation after about 4 hours. Measurements at other temperatures showed that the time constant for gel formation in the observed temperature range (–4 °C to 4 °C) does not significantly depend on the temperature.

Table 1 shows the values for the fit parameters according to eq 1 for gels with gelatin concentrations of 5%, 10% and 20%.

The time constants for the renaturation are subject to a large degree of uncertainty, so that no clear dependence of $\tau$ on the gelatin concentration in the gel can be identified. Furthermore, as expected, the values for $\Delta H_{\text{denat}}^{\max}$ and $\Delta H_{\text{denat}}^{i}$ are statistically not significantly dependent on the gelatin content. It also appears that the gelatin gels measured during the heating-cooling-heating cycle (see Figure 3) before the second heating run were only about 50% renatured.

Table 1. Denaturation and renaturation enthalpy in J/g gelatin after cooling from 50 °C to 1 °C at 5 K/min, and time constants of isothermal renaturation at 1 °C.

| | Gelatin content 5% | Gelatin content 10% | Gelatin content 20% |
|---|---|---|---|
| $\Delta H_{\text{denat}}^{\max}$ | 23.3 ± 0.8 J/g | 25.6 ± 0.6 J/g | 25.2 ± 0.6 J/g |
| $\Delta H_{\text{denat}}^{i}$ | 10.9 ± 0.9 J/g | 9.3 ± 0.9 J/g | 9.0 ± 0.9 J/g |
| $\tau$ at 1 °C | 100 ± 23 min | 77 ± 19 min | 85 ± 22 min |

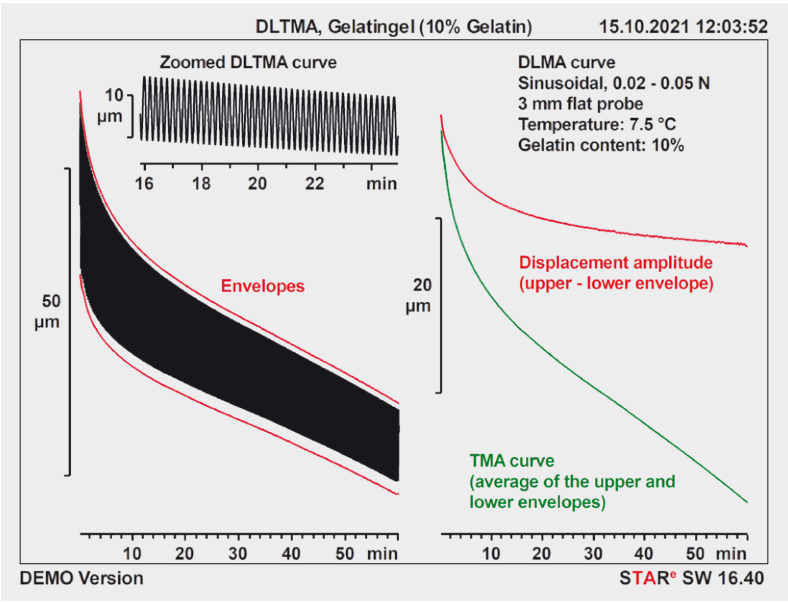


Figure 8. Isothermal renaturation at 7.5 °C. Gelatin content of the gel was 10%.

## TMA measurements of gelatin gels

Gelatins are characterized by their so-called gel strength. Even today, gel strength is still measured using the procedure suggested in 1925 by Oscar T. Bloom. This involves dissolving 7.5 g of gelatin in 105 g water in a standardized glass container at 60 °C and then keeping it for 17 hours at 10 °C. A suitable instrument then determines the mass in grams needed to depress the surface of the gel by 4 mm using a standardized plunger. This mass expressed in grams is the so-called Bloom number [1, 2]. It characterizes a gelatin with a particular gelatin/water ratio (7.5 : 105) which has been subjected to a defined time and temperature program.

The gel strength defined in this way cannot be determined using a TMA.

On the other hand, TMA can be used to investigate both sol to gel, and gel to sol transitions. In the following two sections we describe some possible procedures.

## Gel formation (sol to gel)

To investigate gel formation, 38 mg gelatin gel (gelatin content 10%) was filled into a 100-µL crucible, which was then hermetically sealed. The sample was first heated to 50 °C in the TMA and then cooled to 7.5 °C at 5 K/min. At this temperature, the crucible lid was removed and the sample aged for 5 minutes (applied force –0.1 N, that is, the probe was not in contact with the sample). This was done to make sure that the gel had formed to such an extent that the TMA probe did not penetrate into the gel. The actual measurement was performed in the DLTMA mode in which the sample is subjected to a variable force. In the example described, we used a sinusoidal force that varied between 0.02 and 0.05 N. The measurement curve for this segment is shown in the diagram on the left of Figure 8; the small inset diagram shows a zoomed section of the DLTMA curve. The displacement amplitude of the gel (diagram right, red curve) was then determined from the difference between the upper and lower envelopes of the DLTMA curve (red curves in the diagram on the left). It can be seen the displacement amplitude decreases with increasing time, which means that the strength of the gel increases. The TMA curve can be calculated (green curve in the right diagram) from the average of the upper and lower envelopes. The curve first shows a rapid decrease from which we conclude that gel formation was initially insufficient and that the probe penetrated a little into the gel. At the same time, the thickness of the gel decreases slowly with increasing time, which we interpret as the gel "flowing".

The ratio of the displacement amplitude and the deformed height of the gel (i.e. the TMA curve) can be looked on as a measure of the strength of the gel. This curve is shown in Figure 9 together with a model curve according to the equation:

$$y(t) = y_0 + a_1 \cdot e^{-t/\tau_1} + a_2 \cdot e^{-t/\tau_2} \quad (2)$$

Here y(*t*) is the relative strength of the gel at time *t*, $y_0$ is the maximum relative strength, $a_1$ and $a_2$ are two parameters which correspond to the "strength" of the processes characterized by the time constants $\tau_1$ and $\tau_2$. The values obtained for the time constants were 2.8 min ($\tau_1$) and 22.0 min ($\tau_2$). We think that $\tau_1$ describes the initial penetration of the probe into the insufficiently formed gel, and $\tau_2$ the actual gel formation.

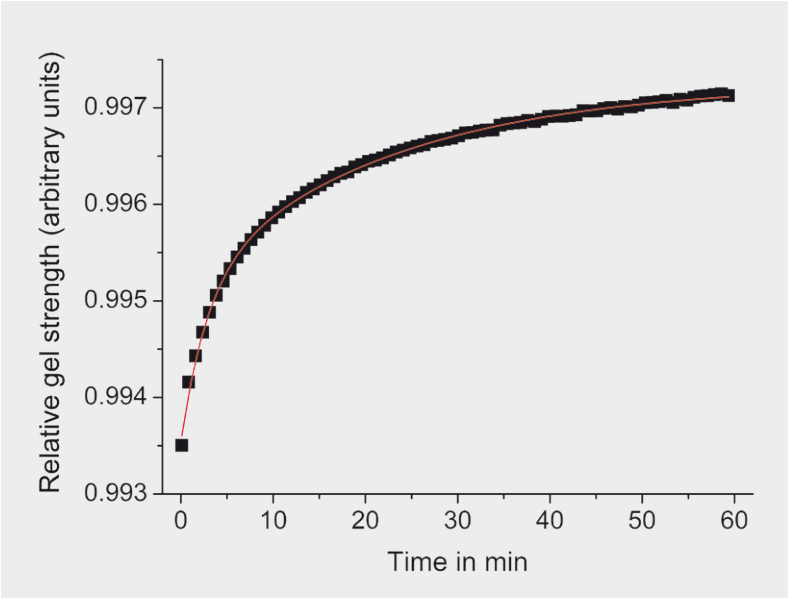


Figure 9.
Relative gel strength at 7.5 °C as a function of time. Gelatin content of the gel is 10%.

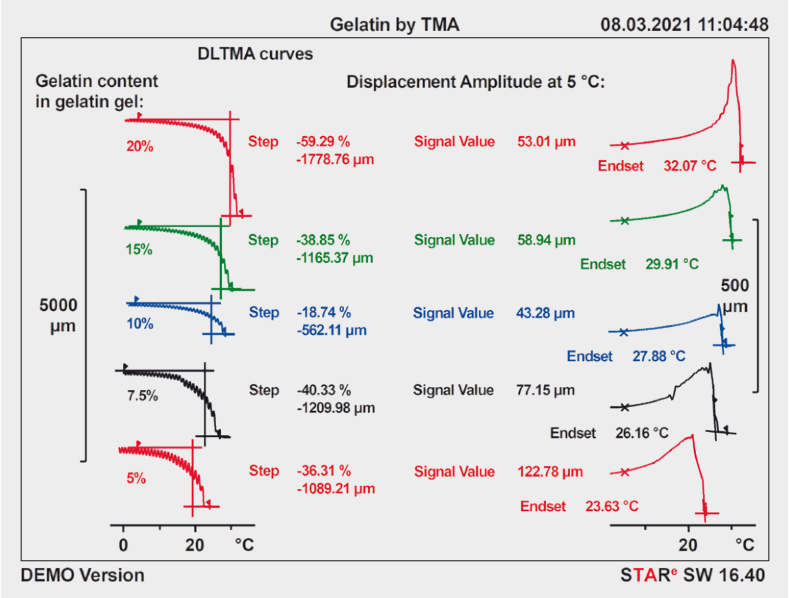


Figure 10.
DLTMA measurements of different gelatin gels.

## Stability of gelatin gels (gel to sol)

In the following experiment, the thermal stability of the same gel samples that had been measured by DSC was investigated. The measurement program was described earlier (see Experimental details). Figure 10 shows the DLTMA curves measured for the different gels and the displacement amplitudes calculated from them. The measurement curves show that

the gels become softer with increasing temperature (displacement amplitude increases) and that the probe penetrates deeper and deeper into the gels. At the given endset temperatures, the gel liquefies (sol) and the probe rests on the bottom of the crucible. The endset temperature increases with increasing gelatin content. Figure 11 shows the endset temperature for the gels as a function of their gelatin content (blue measurement points and dotted curve, linear best fit). The relative strength of the different gels at 5 °C (red measurement points and dotted curve, linear best fit) are also plotted in the diagram. The ratio of the thickness of the gel (step height of the upper envelope) and the displacement amplitude at 5 °C was used as a measure of this. The diagram shows that the so-defined relative gel strength clearly depends on the gelatin content. The results of course depend on the thermal history of the gel.

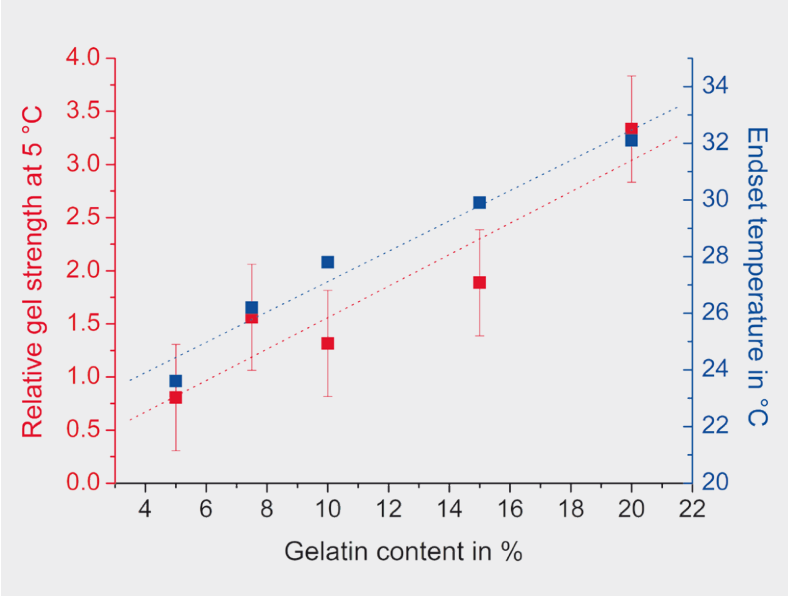


Figure 11.
Relative gel strength and liquefaction temperature (endset temperature) of gelatin gels as a function of their gelatin content. The results depend on the thermal history of the gel.

## Conclusions

A sample of gelatin was investigated using different thermal analysis measurement methods. The water content of the gel, its glass transition temperature and the enthalpy of denaturation determined were determined by DSC and TGA/DSC coupled to a mass spectrometer. Gelatin gels with different contents of gelatin were analyzed by DSC and TMA. Both techniques can be used to investigate sol to gel and gel to sol transformation.

## References

[1] www.sizes.com/units/bloom.htm
[2] Gelatin Handbook, published by the Gelatin Manufacturers Institute of America. www.gelatin-gmia.com/uploads/1/1/8/4/118450438/gmia_gelatin_manual_2019.pdf

**For more information:**
**www.mt.com/ta-techniques**

# Moisture curing of an adhesive using the TMA/SDTA 2+

Dr. Andreas Bach

**In this article, we describe how the moisture curing of an adhesive can be investigated using TMA-Sorption measurements. The isothermal curing behavior of an adhesive at different air humidity levels can be followed in DLTMA experiments by varying the applied force. The gelation time can also be determined.**

## Introduction

The measurement of the gelation time of a thermoset during curing is one of the standard applications of TMA [1]. The gelation time or pot life is the time that the molecules in a resin take to form a gel. After gelation, the resin is no longer suitable for its intended use. The gelation time determines the timeframe in which the resin undergoing curing can be processed. Curing reactions can be initiated by the input of heat, light or moisture. Investigation of the latter means that experiments must be carried out under conditions of controlled humidity. Moisture-curing resins can be investigated by coupling a TMA/SDTA 2+

to a humidity generator. The sample is exposed isothermally to a defined relative humidity (RH) and the sample measured using the DLTMA technique [1].

In this article, we show how the moisture curing of an adhesive can be investigated by DLTMA-Sorption using polyurethane (PUR) as an example.

## Experimental details

The sorption experiments were performed using a TMA/SDTA 2+ coupled to a humidity generator. The setup is shown schematically in Figure 1. The humidity generator generates a gas flow of defined relative humidity. The gas flow (200 mL/min) generated by the humidity generator enters the furnace chamber of the TMA/SDTA 2+ via a humidity interface attached to the outlet of the TMA furnace. A dry gas flow of 10 mL/min that flows round the LVDT is also needed (protective gas). The temperature of the interface must be higher than the condensation temperature of the humidified gas in order to prevent condensation of the humidified gas generated by the humidity generator. For this reason, we recommend the use of two cryostats: one is used to thermostat the LVDT and cool the furnace flange and furnace jacket, and the other to stabilize the temperature of the humidity interface. In these experiments the humidity interface was stabilized at 35 °C.

Figure 2 shows the experimentally determined minimum and maximum relative humidity levels that can be obtained at different temperatures by the TMA/SDTA 2+ combined with a humidity generator system.

The TMA measurements were performed using a 3-mm ball-point probe. The force during the DLTMA measurement varied sinusoidally between –0.010 and 0.010 N with a period of 12 seconds. Sample preparation consisted of putting a small drop of liquid PUR adhesive directly onto the quartz glass sample holder of the TMA at 30 °C.

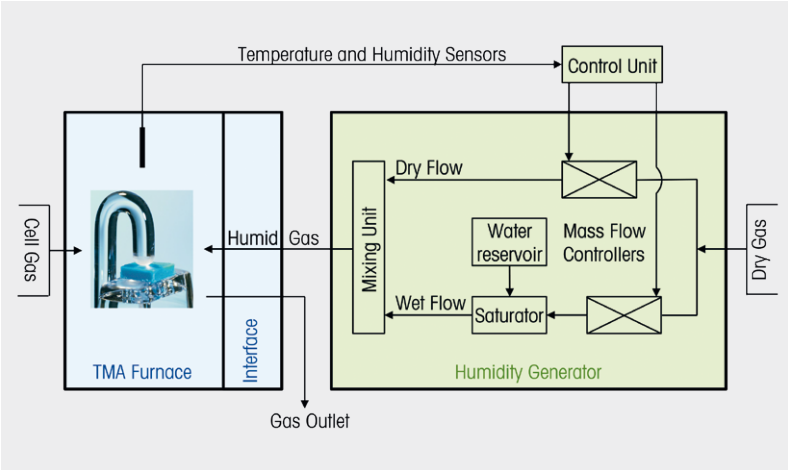


Figure 1.
Setup of a system for sorption experiments using TMA.

After the measurement, the cured sample was burned off with a small flame and the residue brushed away after cooling.

## Results and evaluation

Figure 3 shows the results of a DLTMA measurement performed at 30 °C and a relative humidity of 90%. The lower diagram shows the DLTMA measurement curve. As a result of the sinusoidal change of the applied force, the DLTMA curve also varies sinusoidally between maxima and minima. The Envelope evaluation function joins the minima and maxima together to form two new curves. The upper diagram shows the difference curve of these two curves. It corresponds to the displacement amplitude of the sample due to the influence of the varying force.

In the liquid state, the measurement probe loses contact with the sample under the influence of the negative force (the probe is pressed upward). After about 20 minutes, this effect gradually decreases. Between 70 and 100 minutes the displacement amplitude remains high at a constant level; the measurement probe no longer loses complete contact with the sample.

Apparently, a sticky film or skin has formed on the surface of the droplet, which prevents the measurement probe from leaving the sample. This film forms a "diffusion barrier" between the inside of the PUR sample (material that has not yet cured) and the humid furnace atmosphere so that further curing only occurs very slowly. From 100 minutes onward the displacement amplitude becomes significantly smaller. After about 170 minutes, it is practically zero, the material has become a sticky gel and the sample is

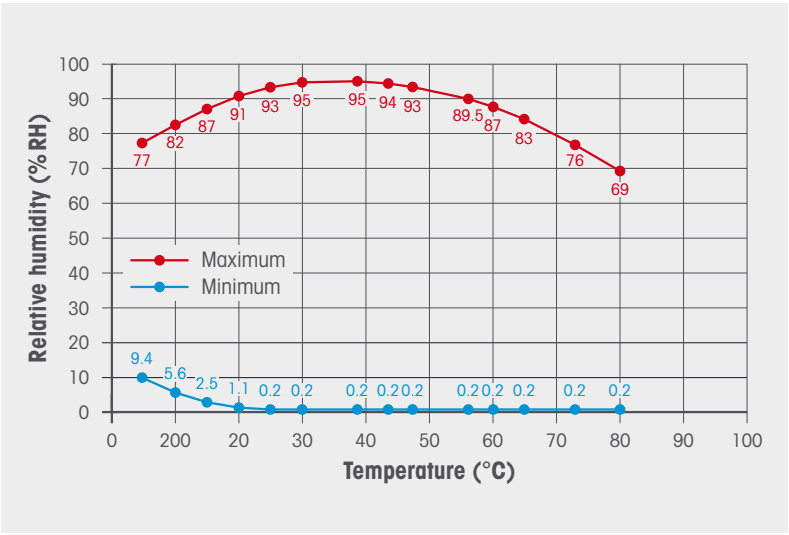


Figure 2.
Minimum and maximum of the relative humidity in the TMA/SDTA 2+ as a function of temperature.

stuck to the measurement probe. The first step, characterized by the onset time T1, describes the formation of a surface film, the second step with the onset T2 the beginning of curing of the whole drop, which after the end time T3 has almost completely cured. T3 therefore corresponds to the gelation time of the sample.

The curing of the PUR adhesive through the action of moisture at 30 °C was also measured at relative humidity levels of 70% and 80%. Figure 4 shows the characteristic times T1, T2 and T3 as a function of the relative humidity. The reaction proceeds more rapidly with increasing relative humidity. The figure shows that surface film formation (T1) and the beginning of the "internal moisturization" of the sample (T2) are much less dependent on the relative humidity than the gelation time T3.

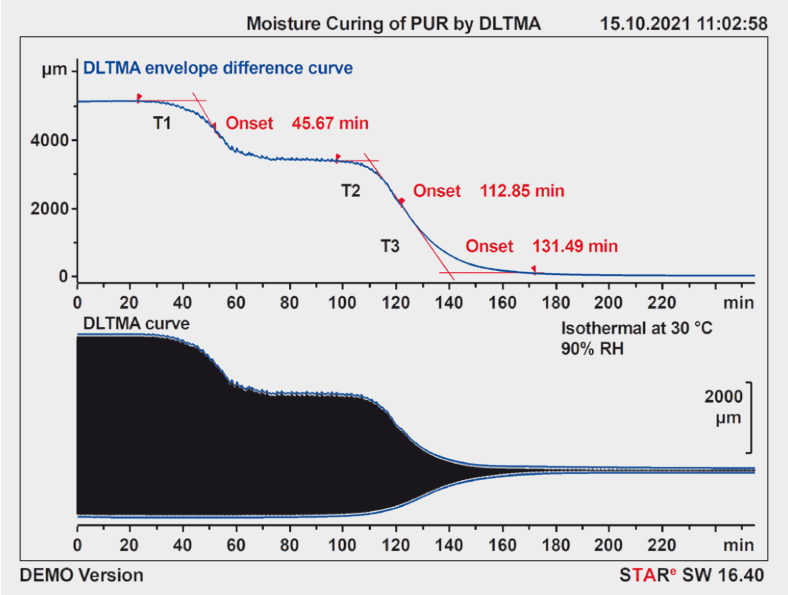


Figure 3. Moisture curing of a polyurethane adhesive at 30 °C and a relative humidity of 90%.

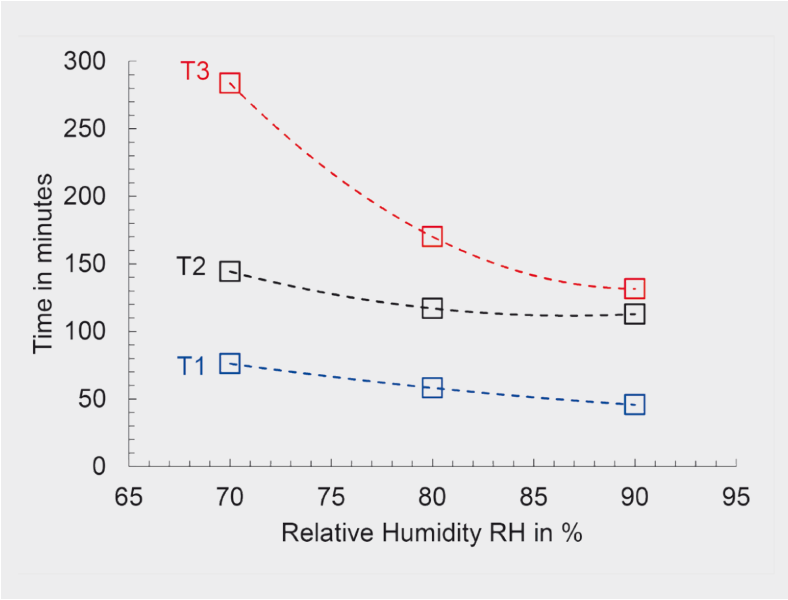


Figure 4. Onsets (T1, T2, and T3) as a function of the relative humidity.

## Conclusions

The TMA/SDTA 2+ combined with a humidity generator is a good technique to use to investigate the sorption and desorption behavior of different materials. This is done by varying the relative humidity in the furnace chamber of the TMA/SDTA 2+ stepwise or continuously under isothermal conditions using a humidity generator.

The moisture curing of a thermoset can be measured by performing DLTMA-Sorption experiments. The gelation time of a PUR adhesive as a function of the relative humidity was determined as an example.

## References

[1] Determination of the gelation time by DLTMA. Thermal Analysis Application No. HB 23. Application published in METTLER TOLEDO TA Application Handbook Thermosets Volume 1.

**For more information:**

**www.mt.com/ta-moisture**

# Reverse engineering of an unknown elastomer

Nicolas Fedelich

**Reverse engineering or deformulation analysis refers to the identification and quantification of individual constituents of a formulated chemical product using different analytical techniques. Deformulation analysis is routinely used by companies to analyze competitors' products and thereby assess the impact of any differences on the performance of a particular product. This article describes how the constituents of an unknown elastomer can be identified and quantified using thermal analysis and other analytical techniques.**

## Introduction

Reverse engineering is widely used in the rubber industry. Companies routinely analyze competitors' products to obtain information about the composition and specifications of products. Elastomer blends contain a large number of additives, including elastomers, plasticizers, inorganic fillers, carbon black, anti-degradants and antioxidants, vulcanizing agents and flame retardants. Some of the additives are present at very low concentrations, which often makes their identification difficult. Vulcanization reactions change the nature of the constituents in an elastomer and make the product more complex. In a competitively oriented market, the rapid introduction of new products with better performance is decisive for any manufacturer. Many different analytical techniques are therefore employed to identify the materials and processes used to produce a particular vulcanized elastomer blend from a mixture of rubbers, polymers, fillers and numerous other additives.

The techniques used for deformulation analysis include thermal analysis, spectroscopy and chromatography. This article shows how thermogravimetric analysis (TGA), differential scanning calorimetry (DSC), dynamic mechanical analysis (DMA) and TGA coupled to a gas chromatography mass spectrometry system (TGA-GC/MS) was used to determine the constituents of an unknown elastomer.

## Materials

The sample was an unknown black elastomeric material.

## Experimental details

### DSC

The DSC experiments were carried out using a METTLER TOLEDO DSC 3+ equipped with a liquid nitrogen cooling accessory and an FRS 6+ sensor. About 10 mg of sample material was heated in a 40-µL aluminum crucible from –150 to 150 °C at 10 K/min.

### DMA

The DMA experiments were carried out using a METTLER TOLEDO DMA/SDTA861$^e$ in the shear mode. The dimensions of the sample were 3 mm (length) × 3 mm (width) × 1.5 mm (thickness). A displacement scan was first performed to determine the linear range of the sample. The sample was then heated from –150 to 100 °C at a heating rate of 2 K/min at frequencies of 1 and 10 Hz. The maximum force and displacement amplitudes were 5 N and 1-µm.

### TGA

The TGA experiments were carried out using a METTLER TOLEDO TGA/DSC 3+ equipped with an STDA sensor. About 15 to 20 mg of sample material was placed in a 70-µL aluminum oxide crucible, heated from 40 to 600 °C and then cooled from 600 to 300 °C in nitrogen at a flow rate of 50 mL/min. At 300 °C the atmosphere was switched to air and the sample heated from 300 to 900 °C.

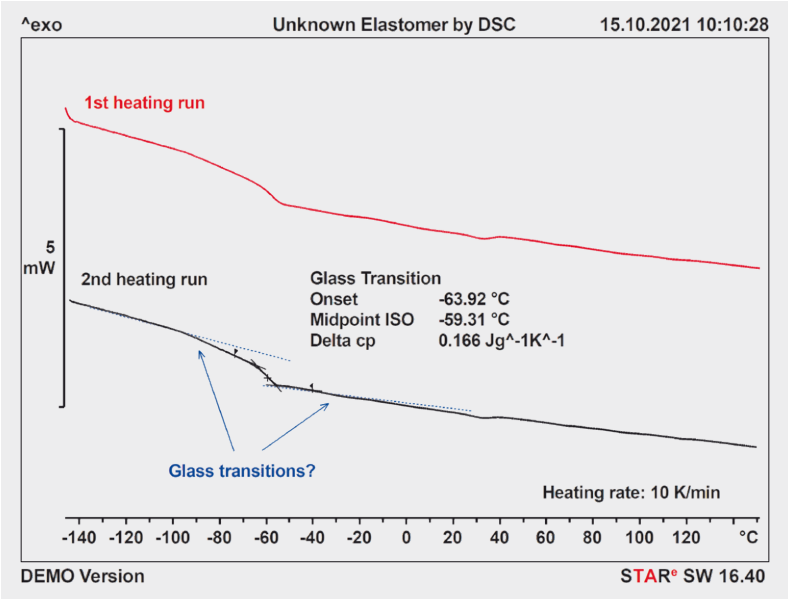


Figure 1.
First and second DSC heating runs of the unknown elastomer.

## ATR

ATR measurements were performed using the built-in ATR unit of the Thermo-Nicolet FTIR iS50. Each spectrum was the average of 32 scans measured at a resolution of 4 $cm^{-1}$ in the range 400 to 4000 $cm^{-1}$.

## TGA-IST-GC/MS

The TGA was coupled to an Agilent gas chromatograph (7890 GC) and an Agilent mass selective detector (5975C MSD) by means of an SRA Instruments IST16 interface. About 20 mg of sample material was heated from 40 to 600 °C at 10 K/min in nitrogen at a flow rate of 50 mL/min. The temperature of the IST16 transfer line and oven was set to 250 °C and the GC split/splitless injector to 280 °C. The temperature program of the GC oven consisted of an isothermal segment at 50 °C for 5 min, followed by heating to 300 °C at 10 K/min, and another isothermal segment at 300 °C for 5 min. The GC column was an HP-5ms (60 m × 0.32 mm × 0.25 µm). Helium was used as carrier gas in the pressure control mode to ensure a column flow of 0.8 mL/min. The helium flow was split in the ratio 5:1 at the GC injector. The mass spectrometer was operated in the scan mode from 33 to 350 m/z using electron impact (EI) ionization at 70 eV and an electron multiplier voltage of 1. The temperature of the ion source was set to 230 °C and that of the quadrupole to 150 °C. The compounds recorded in the GC/MS total ion chromatogram (TIC) were identified using the NIST/EPA/NIH Mass Spectral Library 2011 [3].

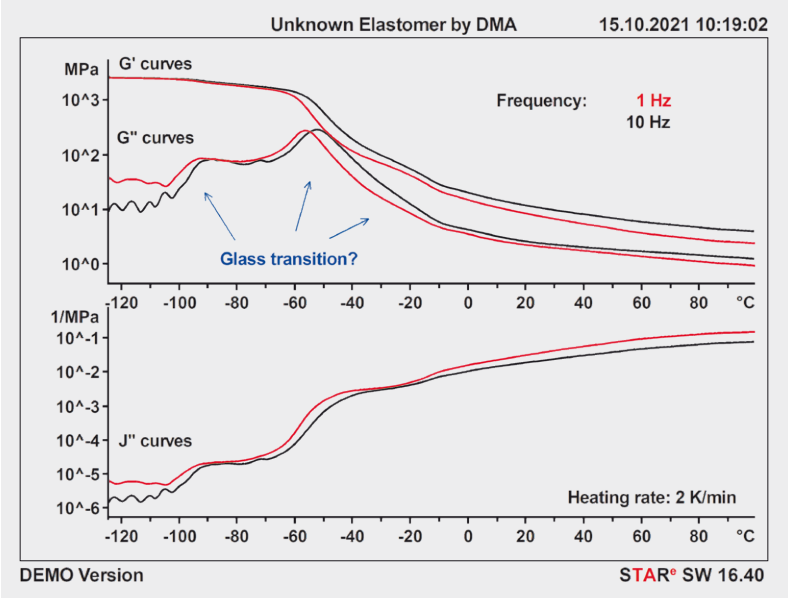


Figure 2.
DMA results (shear mode). Upper diagram: storage modulus (G') and loss modulus (G''). Lower diagram: loss compliance (J'').

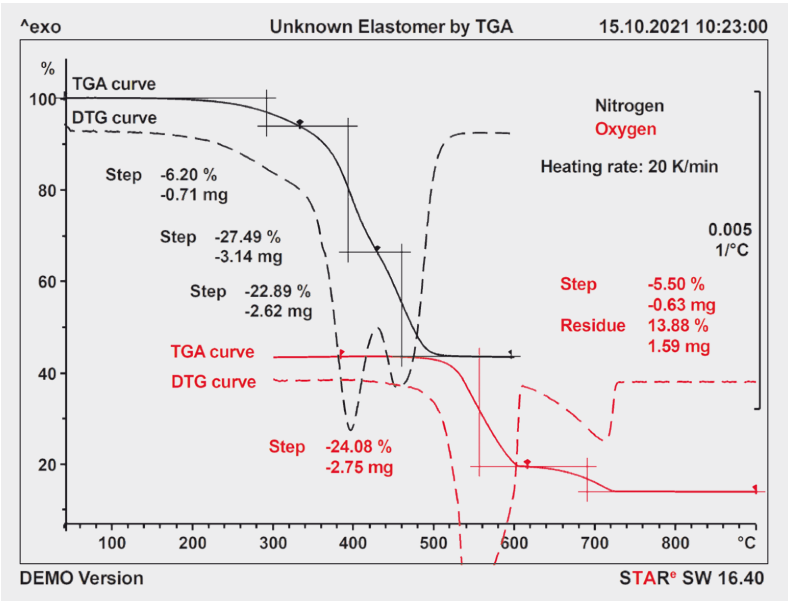


Figure 3.
TGA and DTG curves of the unknown elastomer. The black curves were measured in an inert atmosphere (nitrogen) and the red curves in an oxidative atmosphere (oxygen).

## Results and discussion

### DSC

The DSC results are shown Figure 1. A glass transition can be clearly seen at –60 °C. This could correspond to the glass transition of natural rubber (NR), which typically has its glass transition around this temperature. The DSC curve also shows weak effects marked by the arrows and the dotted lines at about –90 °C and –40 °C. These effects could correspond to the glass transitions of other elastomers. The temperatures are typical for butadiene rubber (BR) and styrene-butadiene rubber (SBR) [1].

### DMA

Figure 2 displays the results of the DMA experiment. The upper part of the diagram shows the storage modulus (G') and loss modulus (G'') curves and the lower part the loss compliance (J'') curve. The red curves were measured at a frequency of 1 Hz and the black curves at 10 Hz. Three effects (marked by the blue arrows) can be seen at –90, –60 and –40 °C. The glass transition at about –60 °C is equally clearly identified as in the DSC curves. Furthermore, the frequency-dependent effect at –90 °C can be assigned to a second glass transition. The effect at –40 °C also seems to be frequency dependent and can likewise be interpreted as a glass transition. The DMA results thus confirm the DSC results.

### TGA

The TGA results are displayed in Figure 3. The TGA curves are shown as solid lines and first derivative curves (DTG) as dashed lines. The black curves were measured in nitrogen and the red curves after switching to oxygen.

The first small weight loss step of about 6% at low temperature is due to the vaporization of volatile compounds. After this, the DTG curve shows two distinct peaks caused by the pyrolysis of the polymeric constituents. The second weight loss step corresponding to the DTG peak maximum at about 370 °C (typical for the pyrolysis of NR) is about 27%. The third weight loss step of about 23% corresponding to the DTG peak maximum at about 440 °C is caused by the pyrolysis of different polymeric components. After switching the atmosphere from nitrogen to oxygen, the TGA heating curve shows a weight loss of 24% at about 550 °C due to the combustion of the carbon black filler. A further weight loss of about 5.5% also occurs at about 650 °C. This probably corresponds to the loss of carbon dioxide produced by the decomposition of a carbonate compound used as a filler.

The inorganic fillers used in the elastomer were identified by recording FTIR-ATR spectra (immediately after the TGA measurement) of the two residues that remained after heating to 600 and 900 °C in air. The resulting IR spectra are shown in Figure 4 (spectra a and b). The residue heated to 900 °C was also left for a few days at room temperature in air before recording a second FTIR-ATR spectrum (c).

The IR spectra of the residues at 600 and 900 °C measured immediately after the TGA analysis show distinct differences. The bands at 1410, 873 and 712 $cm^{-1}$ observed in the IR spectrum of the residue at 600 °C (Figure 4a) are no longer present in the IR spectrum of the residue at 900 °C (Figure 4b). These absorption bands are characteristic of calcium carbonate. The broad band at 1410 $cm^{-1}$ is assigned to the ν3 mode of $CO_3$ (asymmetric stretching vibration). The band at 873 $cm^{-1}$ corresponds to the ν2 mode of $CO_3$ (asymmetric out-of-plane deformation vibration). The band with a maximum at 712 $cm^{-1}$ is due to the ν4 mode of $CO_3$ (symmetric deformation vibration).

| Wavelength in $cm^{-1}$ | Band assignment |
|---|---|
| 1410 | $CO_3$ asymmetric stretching |
| 873 | $CO_3$ asymmetric out-of-plane deformation |
| 712 | $CO_3$ symmetric deformation |
| 1117 | $SO_4$ asymmetric stretching |
| 680, 615 and 595 | $SO_4$ asymmetric deformation |
| 3640 | O–H bond |

Table 1. Assignment of bands in the IR spectra of the TGA residues.

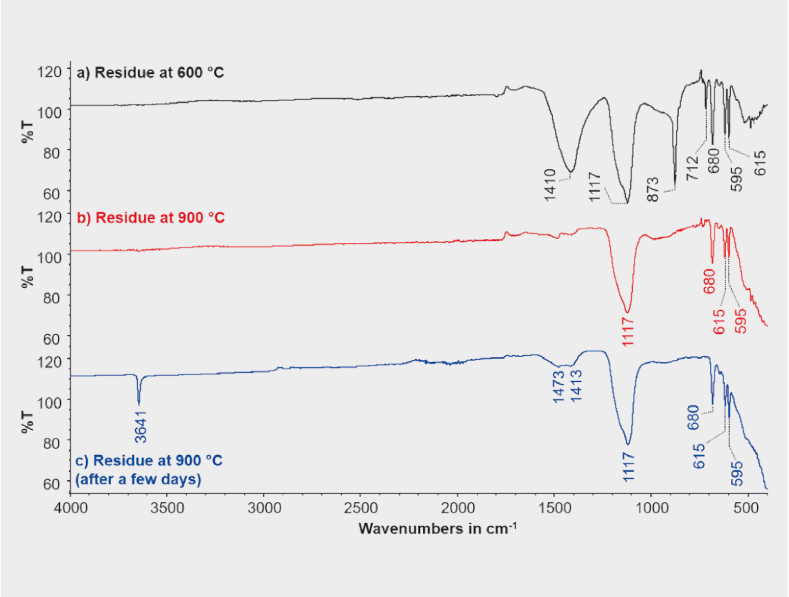


Figure 4. IR spectra of the residues: a) at 600 °C; b) at 900 °C immediately after the TGA analysis and c) at 900 °C after the residue had been left at room temperature in air for a few days.

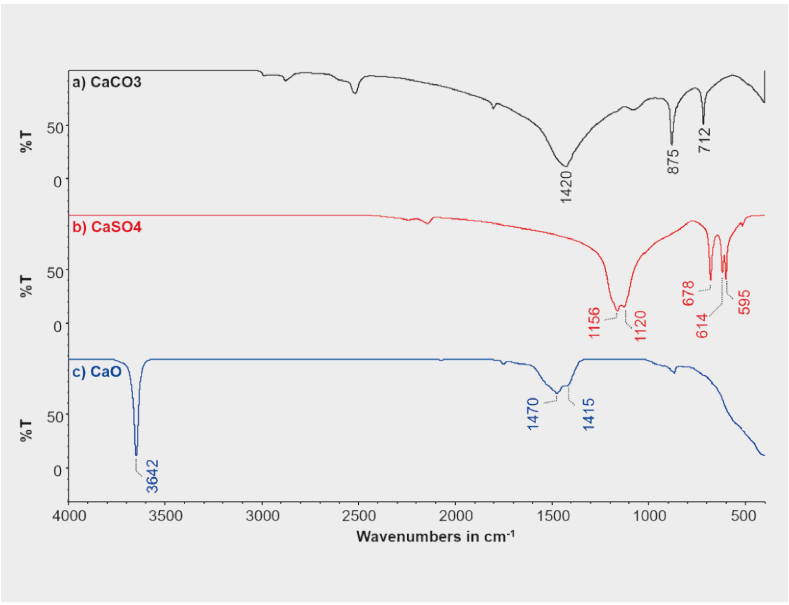


Figure 5. Reference IR spectra: a) $CaCO_3$; b) $CaSO_4$ and c) CaO.

The IR spectrum of the residue at 900 °C that had been left for a few days at room temperature (Figure 4c) shows a sharp band at 3640 $cm^{-1}$. This corresponds to the O–H-bond of calcium hydroxide, $Ca(OH)_2$, present at a low concentration in the sample. The hydroxide is a residue from the carbonation process occurring in the sample. This is also shown by the recurrence of the broad band at about 1410 $cm^{-1}$, which corresponds to the ν3 mode of $CO_3$.

| IST Loop number | 2 | 3 | 4 | 5 | 6 | 7 | 8 | 9 | 10 | 11 | 12 | 13 | 14 | 15 | 16 |
|---|---|---|---|---|---|---|---|---|---|---|---|---|---|---|---|
| TGA temp. in °C | 160 | 200 | 230 | 260 | 300 | 310 | 330 | 350 | 370 | 390 | 410 | 430 | 450 | 470 | 550 |

Table 2. Loop numbers and the furnace temperatures at which gas samples were collected and stored in the storage loops of the IST16 storage interface.

The fourth step observed in the TGA curve at about 650 °C is therefore due to the decarboxylation of $CaCO_3$ ($CaCO_3 \leftrightarrow CaO + CO_2$). Based on the stoichiometry on the decomposition reaction, the sample contains about 12.3% $CaCO_3$. This means that the rest of the sample at 900 °C contains about 6.9% calcium oxide. The residual mass without CaO (from the $CaCO_3$) is about 5.5%. Four other peaks are observed in the residues at 600 °C and 900 °C namely at 1117, 680, 615 and 595 $cm^{-1}$. These are characteristic of calcium sulfate ($CaSO_4$). The broad band at 1117 $cm^{-1}$ corresponds to the ν3 mode of $SO_4$ (asymmetric stretching vibration). The three sharp bands with maxima at 680, 615 and 595 $cm^{-1}$ correspond to the ν4 mode of $SO_4$ (asymmetric deformation vibration).

A summary of the band assignments is given in Table 1. Reference IR spectra of $CaCO_3$, $CaSO_4$ and CaO are shown in Figure 5 (spectra a, b and c).

To quantify the $CaSO_4$ content in the elastomer, another specimen was analyzed by TGA using the same method as described above except that it was heated to 1600 °C. The inset diagram in Figure 6 shows the decomposition from about 1200 °C onward. This is characteristic of the decomposition of calcium sulfate, which occurs in several steps. The stoichiometry of the decomposition reaction ($CaSO_4 \rightarrow CaO + SO_2 + ½\ O_2$) yields a $CaSO_4$ content of about 4.4% and means that the CaO originating from the $CaSO_4$ is about 1.8%. At 1600 °C, the total amount of CaO (from the $CaCO_3$ and $CaSO_4$) is 8.7%.

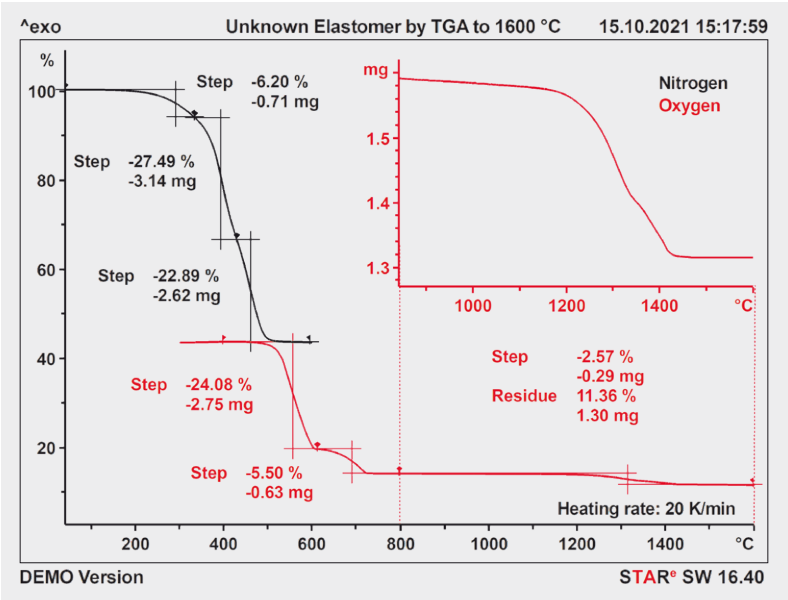


Figure 6.
TGA curves of the unknown elastomer recorded up to 1600 °C.
The black curves were measured in an inert atmosphere (nitrogen) and the red curves in an oxidative atmosphere (oxygen).

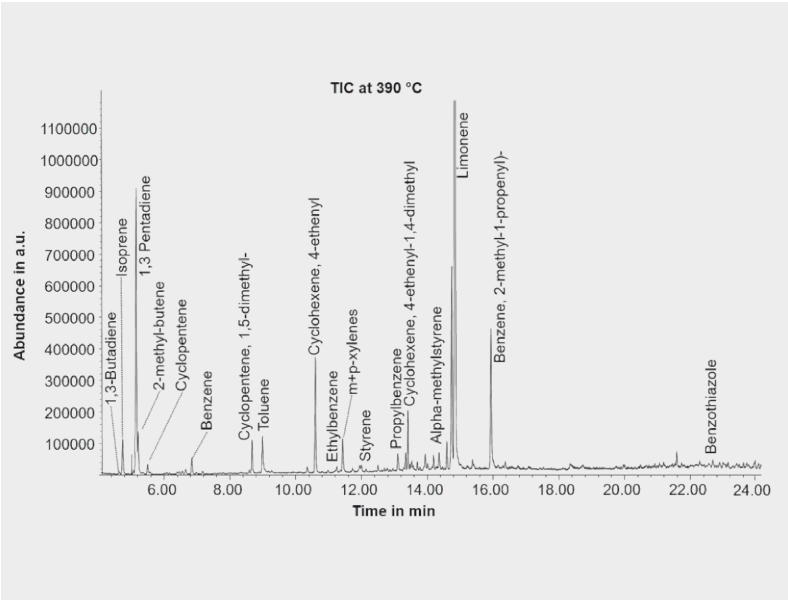


Figure 7.
Total ion current (TIC) chromatogram of the gas sample taken at 390 °C.

## TGA-IST-GC/MS

To identify the individual elastomers in the unknown sample, the TGA was coupled to a gas chromatography-mass spectrometer (GC/MS) system by means of the IST heated storage interface (IST) [2]. The temperatures at which gas samples were collected and stored (see Table 2) were based on the curves recorded in the TGA experiment (Figure 3).

After the last gas sample had been collected in Loop 16, the contents of each loop were injected individually into the GC. Figure 7 for example, displays the total ion chromatogram (TIC) of the contents of Loop 11 collected at a TGA furnace temperature of 390°C. Some of the main peaks identified using the NIST MS library are labeled in the TIC chromatogram. An example of identification is shown in Figure 8. The upper part of the diagram shows the mass spectrum (in blue) of the peak detected just before 14.4 minutes.

The lower part of the diagram shows the reference mass spectrum (in black) of alpha-methylstyrene from the library. This is the best match with a search quality factor of 91. Altogether, about 80 volatile compounds were evolved during the pyrolysis of the unknown elastomer under nitrogen. Some of the more interesting compounds identified are summarized in Table 3 with their main fragment ion masses (m/z), chemical formulas and structure. If the evaluation is carried out for all the loops, curves showing the emission profiles of selected compounds can be plotted as shown in Figure 9.

The presence of isoprene and limonene in the decomposition gases evolved clearly confirms that natural rubber (NR) is one of the constituents of the unknown elastomer. NR is mainly responsible for the first decomposition step as shown by the emission profile of limonene in Figure 9.

The presence of butadiene rubber (BR) and styrene-butadiene rubber (SBR), which was suggested as a result of the DSC and DMA measurements, is confirmed by the TGA-GC/MS results. This is supported by the identification of 1,3-pentadiene for BR and styrene for SBR. In fact, BR and SBR seem to contribute to both decomposition steps (between 300 and 500 °C), which makes it difficult to quantify the three rubber constituents.

Another interesting compound identified was benzothiazole. This is the main decomposition product of mercaptobenzothiazole, which is present in the sample as a vulcanization accelerator. It indicates that sulfur was used to vulcanize the rubber. The TGA-GC/MS results are summarized in Table 4.

The results of the different experiments indicate that the unknown elastomer is a ternary blend of NR, BR and SBR. These three elastomers constitute about 50% of the sample. The sample also contains about 6% volatile substances. Sulfur was used as vulcanizing agent

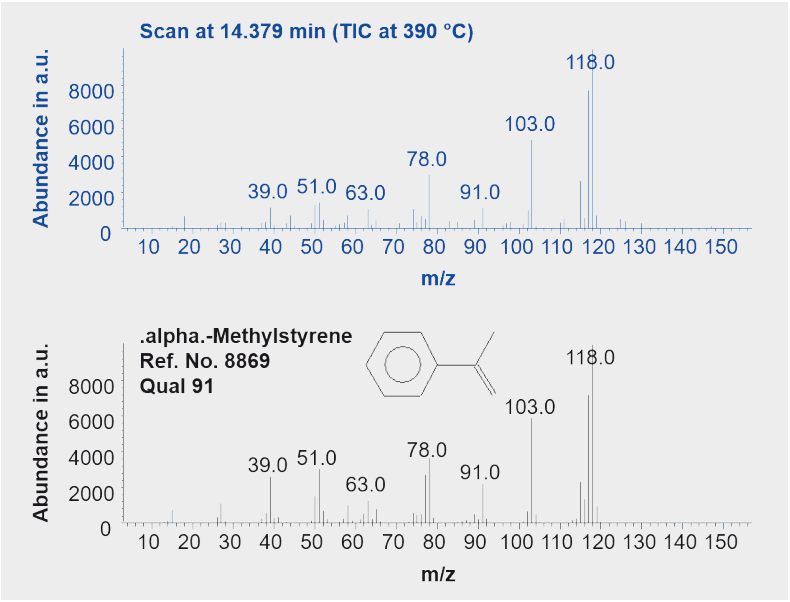


Figure 8.
Example of the identification of a TIC peak using the NIST MS database.

| Compound name | Main (m/z) | Formula | Structure |
|---|---|---|---|
| 1,3-butadiene | 54 | $C_4H_6$ | |
| Isoprene | 67 | $C_5H_8$ | |
| 1,3-pentadiene | 68 | $C_5H_8$ | |
| Benzene | 78 | $C_6H_6$ | |
| Toluene | 91 | $C_7H_8$ | |
| Cyclohexene, 4-ethenyl (butadiene dimer) | 54 | $C_8H_{12}$ | |
| Ethylbenzene | 91 | $C_8H_{10}$ | |
| m-xylene | 91 | $C_8H_{10}$ | |
| Styrene | 104 | $C_8H_8$ | |
| Propylbenzene | 120 | $C_9H_{12}$ | |
| Alpha-methylstyrene | 118 | $C_9H_{10}$ | |
| Limonene (racemate) | 68 | $C_{10}H_{16}$ | |
| Benzothiazole | 135 | $C_7H_5NS$ | |

Table 3.
Some of the main compounds identified in the TGA-GC/MS analysis.

and the sample was filled with about 24% carbon black. The inorganic fillers are calcium carbonate (about 12%) and calcium sulfate (about 4%).

More comprehensive reverse engineering of the sample would require the use of additional techniques such as ultraviolet spectroscopy (UV), nuclear magnetic resonance (NMR), atomic absorption (AA), high performance liquid chromatography (HPLC), thin layer chromatography (TLC) and others. For example, after decomposition of the elastomer in an oxygen-free atmosphere, the type of carbon black could be determined by measuring its particle size using transmission electron microscopy (TEM).

Table 4.
Summary of the TGA-GC/MS results.

| Selected compounds | Source |
|---|---|
| Limonene, isoprene and m-xylene | Natural rubber (NR) |
| 1,3-pentadiene and 4-ethenylcyclohexene | Butadiene rubber (BR) |
| Propylbenzene, styrene and α-methylstyrene | Styrene-butadiene rubber (SBR) |
| 1,3-butadiene | BR and SBR |
| Toluene | NR, BR and SBR |
| Benzothiazole | 2-mercaptobenzothiazole (vulcanizing agent) |

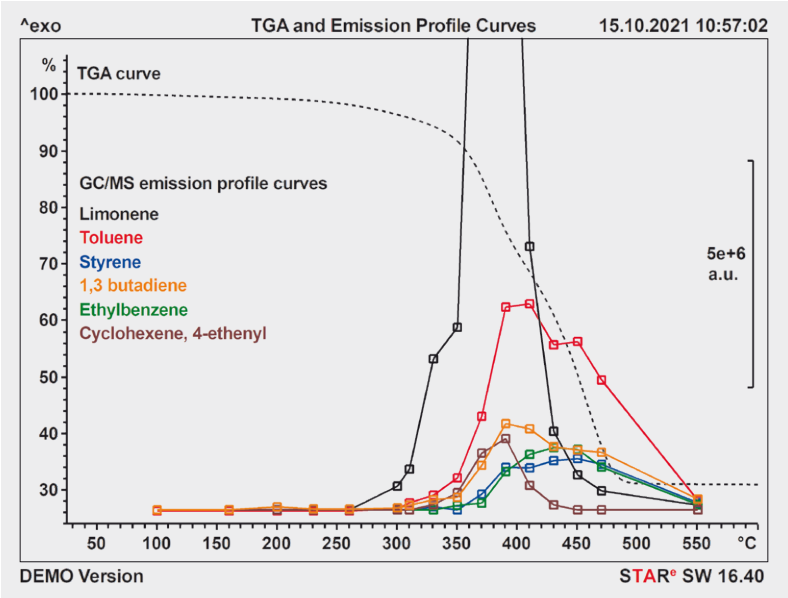


Figure 9.
TGA curve (left axis) and curves showing the emission profiles of several relevant compounds (right axis).

## Conclusions

This article shows how thermal analysis and other techniques were used to identify constituents of an unknown elastomer. The contents of volatile substances, elastomers, carbon black and inorganic fillers were determined. The results obtained using a TGA coupled to an IST16/GC/MS system allowed us to conclude that the unknown elastomer was based on a ternary blend of NR, SBR and BR.

## References

[1] J.E.K. Schawe, METTLER TOLEDO Collected Applications Handbook: ELASTOMERS, Volume 2, 171.
[2] N. Fedelich, Thermogravimetric analysis and gas analysis Part 4: TGA-GC/MS, UserCom 48, 1–7.
[3] N. Fedelich, A novel TG-GC/MS system, Quantification of low-content styrene-butadiene rubber in natural rubber, J. Therm. Anal. Calorim (2017) 127: 947–954.

**For more information:**
**www.mt.com/ta-ega**

# Influence of sample volume in the high-pressure crucible on the DSC signal

Dr. Kai Hassdenteufel

**High-pressure DSC crucibles are widely used for safety studies of reactive substances. In this application, very small amounts of sample are used. On the other hand, chemical reactions are measured in sealed crucibles in order to suppress the formation of gas or the vaporization of solvents. In this case, the sample volumes are large. The influence of sample volume on the heat flow signal in the METTLER TOLEDO gold-plated high-pressure crucibles is demonstrated using the melting peak of indium.**

## Introduction

High-pressure crucibles are mainly used in safety studies of reactive substances, for example for the analysis of explosive substances and propellants. For safety reasons, in applications like this, only small amounts of sample (typically less than a milligram) are used. In contrast, large sample volumes have to be used to study chemical reactions with low reaction enthalpies in order to obtain an adequate signal. The advantage of a measurement at constant volume is that no work of expansion is required, which means that chemical reactions are measured free of evaporation, vaporization and or other types of gas formation. For example, polycondensation reactions, which are usually relatively weak, can be easily measured.

## Experimental details

The sample used for this study was an indium pellet (purity 99.999%, supplier impag), the same as that used for the temperature calibration and adjustment of DSC instruments. To investigate the influence of sample volume, the indium pellet was measured in two different ways in the high-pressure crucible.

First, the indium pellet was placed alone on the bottom of a high-pressure crucible (standard procedure); the sample volume is small, about 1 µL. Measurements showed that indium does not form an alloy with gold at temperatures up to 220 °C. The possibility of alloy formation must be checked beforehand in a trial experiment when measurements are performed with reference substances that melt at higher temperatures.

Second, to simulate a large sample volume, the crucible was first filled to about one third with an inert powder ($Al_2O_3$). The indium pellet was then placed in the middle and the crucible filled to two thirds with $Al_2O_3$ powder. This corresponds to a sample volume of about 25 µL. The idea was that this should produce a heat flow signal corresponding to that from a sample of large volume. The crucibles were sealed using a toggle press. The temperature program consisted of heating the sample four times from 100 to 220 °C at heating rates of 30, 5, 10 and 20 K/min. The purpose of the first heating run was to make good thermal contact between the sample and the crucible. The sample was cooled at 30 K/min between the heating segments (see Figure 1).

The measurements were performed using an air-cooled DSC 1 with FRS 5 sensor. In addition, a standard adjustment of temperature, heat flow and tau-lag was performed on the instrument for the high-pressure crucible used. Afterward, the same measurement was repeated four times for each sample volume. The crucible was inserted manually each time to check the reproducibility of the measurement results.

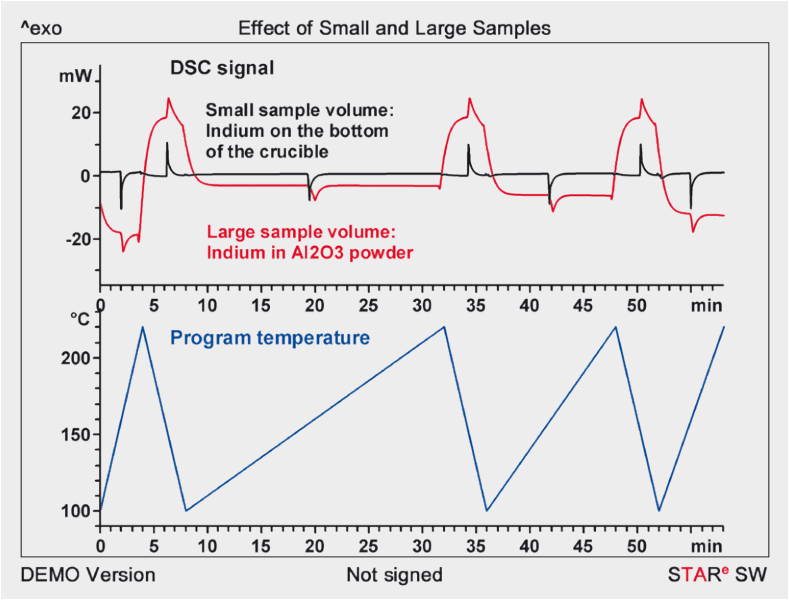


Figure 1.
DSC curves of indium in the high-pressure crucible. Black curve, above: Indium pellet was placed on the bottom of the crucible. Red curve, above: Indium was placed in $Al_2O_3$ powder – the large initial deflections are due to the large heat capacity of the large volume sample. The lower curve shows the temperature profile.

## Measurement results for the high-pressure crucible, standard adjustment

### Evaluation

Figure 2 shows the evaluation of the curves. With the large sample volume, the onset temperature of the melting peak of indium is shifted to higher temperature. The reason for this is the high thermal resistance between the sample and the crucible. This crucible must therefore not be used for the temperature adjustment (with real samples with large volumes thermal effects occur uniformly distributed over the volume itself; they are in direct contact with the bottom of the crucible).

Large initial deflections occur due to the high heat capacity of the $Al_2O_3$ powder.

The measured peak area is on average about 7% smaller when the pellet is in the middle of the $Al_2O_3$ powder. The heating rate has no influence on the measured melting peak area. The results of the evaluations are summarized in Table 1.

### Recommendations for adjustment

To adjust the furnace temperature for both large and small sample volumes, we recommend that you perform a standard adjustment with an indium pellet on the bottom of the high-pressure crucible. This gives the best accuracy for different sample volumes. The dependence of the onset temperature on the heating rate can easily be corrected for corresponding sample volumes using a tau-lag adjustment. To do this, the onset temperatures of the melting peak are plotted against the heating rate; afterward a regression line y = m*x + b is calculated. The intercept with the axis, b, corresponds to the extrapolated onset for a hypothetical heating rate of 0 K/min. This value is used for the temperature adjustment. The slope of the regression line, m, corresponds to the correction value of the tau lag, that is, the time that the sample temperature lags behind the furnace temperature.

The influence of the sample volume can be corrected by adjusting the heat flow. To do this, a new high-pressure crucible was defined in the STARe database for the analysis of samples with large sample volumes. This was given the name "HP gold plated (40 µL), large sample volume" to distinguish it from the standard high-pressure crucible in the STARe software stored under the name "HP Gold plated (40 µL)". Heat flow adjustment for the crucible of large sample volume was then performed. To check the effect of the changes, the two crucibles were measured once again after corresponding adjustment using the same method as described before (Figure 3). The evaluation of the DSC curves now gives a correct enthalpy of fusion for small and large sample volumes.

The mean of four measurements was used for the adjustment of the onset and the melting peak area of indium. The calculated error corresponds to the standard deviation of these values. A single measurement was performed after the adjustment as a check.

| Small sample volume, standard adjustment | | | |
|---|---|---|---|
| Heating rate [K/min] | 5 | 10 | 20 |
| Onset [°C] | 156.58 | 156.71 | 156.93 |
| Standard deviation Onset [K] | 0.05 | 0.08 | 0.18 |
| Peak area (Integral) [J/g] | 28.34 | 28.56 | 28.28 |
| Standard deviation Integral [J/g] | 0.21 | 0.34 | 0.44 |

| Large sample volume, standard adjustment | | | |
|---|---|---|---|
| Heating rate [K/min] | 5 | 10 | 20 |
| Peak area (Integral) [J/g] | 26.63 | 26.26 | 26.42 |
| Standard deviation Integral [J/g] | 0.20 | 0.32 | 0.49 |

Table 1.
Results of the measurements for a small sample volume (indium on the bottom of the high-pressure crucible) and for a large sample volume (indium between two layers of $Al_2O_3$ powder) before and after the adjustment.

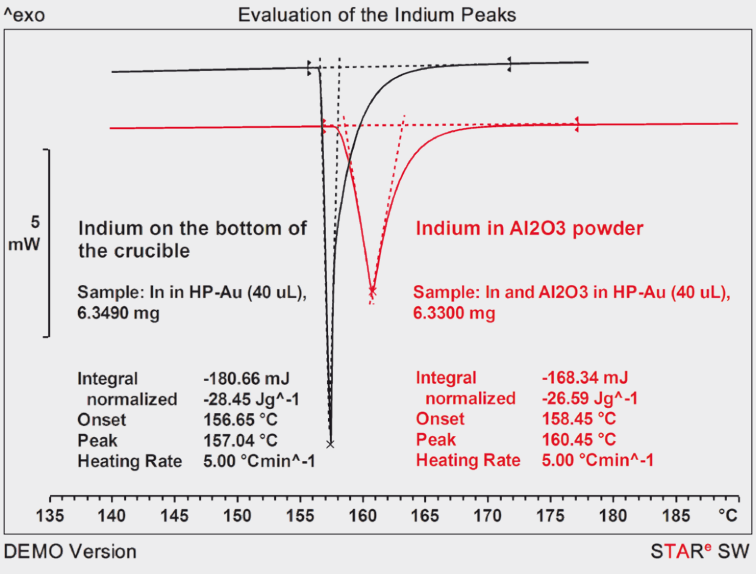


Figure 2.
Comparison of the melting curves of indium for the small and large sample volumes. The peak from the measurement in which the indium pellet was in the middle of the $Al_2O_3$ powder sample is significantly broader. The onset is shifted by about 1.5 K to higher temperature at a heating rate of 5 K/min due to the thermal resistance of the $Al_2O_3$ powder.

## Conclusions

The influence of the sample volume on the heat flow signal in the high-pressure crucible (40 µL, gold-plated) was investigated. In one experiment, an indium pellet was placed directly on the bottom of the crucible to simulate a small sample volume. In a second experiment, an indium pellet was placed between two layers of $Al_2O_3$ powder to simulate a sample of large volume. The

measured melting peak area of the indium is about 7% smaller for the large sample volume (about 25 µL) than for the small sample volume.

The influence of the sample volume can be corrected by adjusting the heat flow. This is done by simulating a sample volume close to that of the sample that is later to be measured. In order to analyze both small and large sample volumes with high accuracy, for small sample volumes we recommend that you adjust the high-pressure crucible using the standard method, that is, with an indium pellet on the bottom of the crucible. For the analysis of samples with large sample volumes, another high-pressure crucible is defined in the STAR$^e$ database, e.g. "HP gold plated (40 µL), large sample volume". The heat flow is then adjusted for both crucibles as described in the above example. This procedure takes the effect of sample volume into account.

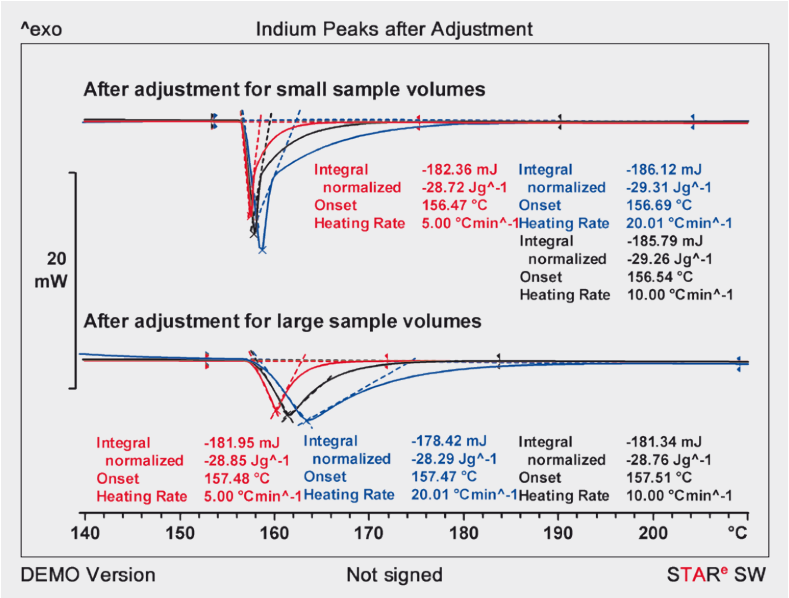


Figure 3.
DSC curves of the high-pressure crucibles with small and large sample volumes after heat flow adjustment was performed. The evaluation now gives a correct enthalpy of fusion for small and large sample volumes.

The best temperature accuracy for samples with small and large volumes is obtained when the furnace temperature is adjusted in the usual way with an indium pellet on the bottom of the high-pressure crucible.

**For more information:**
**www.mt.com/ta-hpdsc**

# Exhibitions, Conferences and Seminars

| | | |
|---|---|---|
| **Green Plast** | May 3–6, 2022 | Milan (Italy) |
| **Analytica** | June 21–24, 2022 | Munich (Germany) |
| **Virtual NATAS (North American Thermal Analysis Society)** | August 2–6, 2022 | Cleveland, OH (USA) |
| **Materials Science & Technology** | October 9–13, 2022 | Pittsburgh, PA (USA) |
| **CAMX** | October 17–20, 2022 | Anaheim, CA (USA) |
| **K 2022** | October 19–26, 2022 | Dusseldorf (Germany) |
| **CAMX** | October 17–20, 2022 | Anaheim, CA (USA) |
| **Materials Science & Technology** | October 9–13, 2022 | Pittsburgh, PA (USA) |
| **MRS Fall Meeting** | November 27–December 2, 2022 | Boston, MA (USA) |

| | | |
|---|---|---|
| **Webinars** | For information on our current program of webinars, please visit | **www.mt.com/ta-webinars**<br>**www.mt.com/ta-ondemand** |
| **Handbooks** | Our specialist application handbooks provide valuable background information | **www.mt.com/ta-handbooks** |
| **Applications** | The applications database includes hundreds of interesting examples | **www.mt.com/ta-applications** |
| **Training courses** | Improve your knowledge of thermal analysis | |
| | • have a look at our extensive training program | **www.mt.com/ta-training** |
| | • or register for an online e-training course | **www.mt.com/ta-etraining** |
| | • or check our training videos | **www.mt.com/ta-videos**<br>**www.mt.com/ta-techniques** |
| **TA News** | You can find the latest product news and an overview of our thermal analysis services at | **www.mt.com/ta-news** |
| **TA Services** | METTLER TOLEDO offers comprehensive support to ensure you get reproducible results in day-to-day analysis | **www.mt.com/ta-services**<br>**www.mt.com/ta-gtap** |
| **Tip: TA Knowledge** | Sign up for the quarterly Thermal Analysis Knowledge Newsletter | **www.mt.com/ta-knowledge** |

# International and Swiss TA Customer Courses

**Q1/2022**

| Course ID and Topic | Date 1 | Online Time (EU/Americas) | Course ID and Topic | Date 2 | Online Time (EU/Asia) | Onsite (EU) |
|---|---|---|---|---|---|---|
| | | CET 14–18 (USA 8–12) | | | CET 8–12 (Asia 14–18) | CET |
| TAK06 SW Basic | February 07, 2022 | 14–18 | TAK06 SW Basic | February 14, 2022 | 8–12 | 8–16 |
| TAK06 TMA | February 07, 2022 | 14–18 | TAK06 TMA | February 14, 2022 | 8–12 | 8–16 |
| TAK06 DMA Basic | February 07, 2022 | 14–18 | TAK06 DMA Basic | February 14, 2022 | 8–12 | 8–16 |
| TAK06 Administration | February 08, 2022 | 14–18 | TAK06 Administration | February 15, 2022 | 8–12 | 8–16 |
| TAK06 DMA Advanced | February 08, 2022 | 14–18 | TAK06 DMA Advanced | February 15, 2022 | 8–12 | 8–16 |
| TAK06 TGA Basic | February 08, 2022 | 14–18 | TAK06 TGA Basic | February 15, 2022 | 8–12 | 8–16 |
| TAK06 TGA Advanced | February 09, 2022 | 14–18 | TAK06 TGA Advanced | February 16, 2022 | 8–12 | 8–16 |
| TAK06 DSC Basic | February 09, 2022 | 14–18 | TAK06 DSC Basic | February 16, 2022 | 8–12 | 8–16 |
| TAK06 DSC Advanced | February 10, 2022 | 14–18 | TAK06 DSC Advanced | February 17, 2022 | 8–12 | 8–16 |
| TAK06 TGA-FTIR | February 10, 2022 | 14–18 | TAK06 TGA-FTIR | February 17, 2022 | 8–12 | 8–16 |
| TAK06 TGA-GC/MS | February 10, 2022 | 14–18 | TAK06 TGA-GC/MS | February 17, 2022 | 8–12 | 8–16 |
| TAK06 SW Advanced | February 11, 2022 | 14–18 | TAK06 SW Advanced | February 18, 2022 | 8–12 | 8–16 |
| TAK06 TGA-MS | February 11, 2022 | 14–18 | TAK06 TGA-MS | February 18, 2022 | 8–12 | 8–16 |
| TAK06 TGA-Micro GC/MS | February 11, 2022 | 14–18 | TAK06 TGA-Micro GC/MS | February 18, 2022 | 8–12 | 8–16 |
| TAK06 Kinetics / TMDSC | February 11, 2022 | 14–18 | TAK06 Kinetics / TMDSC | February 18, 2022 | 8–12 | 8–16 |

**Q3/2022**

| | | | | | | |
|---|---|---|---|---|---|---|
| TAK06 SW Basic | September 05, 2022 | 14–18 | TAK06 SW Basic | September 12, 2022 | 8–12 | 8–16 |
| TAK06 TMA | September 05, 2022 | 14–18 | TAK06 TMA | September 12, 2022 | 8–12 | 8–16 |
| TAK06 DMA Basic | September 05, 2022 | 14–18 | TAK06 DMA Basic | September 12, 2022 | 8–12 | 8–16 |
| TAK06 Administration | September 06, 2022 | 14–18 | TAK06 Administration | September 13, 2022 | 8–12 | 8–16 |
| TAK06 DMA Advanced | September 06, 2022 | 14–18 | TAK06 DMA Advanced | September 13, 2022 | 8–12 | 8–16 |
| TAK06 TGA Basic | September 06, 2022 | 14–18 | TAK06 TGA Basic | September 13, 2022 | 8–12 | 8–16 |
| TAK06 TGA Advanced | September 07, 2022 | 14–18 | TAK06 TGA Advanced | September 14, 2022 | 8–12 | 8–16 |
| TAK06 DSC Basic | September 07, 2022 | 14–18 | TAK06 DSC Basic | September 14, 2022 | 8–12 | 8–16 |
| TAK06 DSC Advanced | September 08, 2022 | 14–18 | TAK06 DSC Advanced | September 15, 2022 | 8–12 | 8–16 |
| TAK06 TGA-FTIR | September 08, 2022 | 14–18 | TAK06 TGA-FTIR | September 15, 2022 | 8–12 | 8–16 |
| TAK06 TGA-GC/MS | September 08, 2022 | 14–18 | TAK06 TGA-GC/MS | September 15, 2022 | 8–12 | 8–16 |
| TAK06 SW Advanced | September 09, 2022 | 14–18 | TAK06 SW Advanced | September 16, 2022 | 8–12 | 8–16 |
| TAK06 TGA-MS | September 09, 2022 | 14–18 | TAK06 TGA-MS | September 16, 2022 | 8–12 | 8–16 |
| TAK06 TGA-Micro GC/MS | September 09, 2022 | 14–18 | TAK06 TGA-Micro GC/MS | September 16, 2022 | 8–12 | 8–16 |
| TAK06 Kinetics / TMDSC | September 09, 2022 | 14–18 | TAK06 Kinetics / TMDSC | September 16, 2022 | 8–12 | 8–16 |

**Information and Course Registration / Auskunft und Registration bei:** Mrs Perla Irmler (or Mrs Veronica Feroce-Ring), Mettler-Toledo GmbH, Analytical, Nänikon
Tel: ++41 44 806 73 57, Fax: ++41 44 806 72 60, e-mail: perla.irmler@mt.com (or veronica.feroce-ring@mt.com)

## Local TA Customer Courses

**Schweiz/Deutschland**
TA-Kundenkurse und Seminare

| Nähere Informationen unter www.mt.com/labtalk oder durch: Frau Janine Schindler, Mettler-Toledo GmbH, Giessen, Tel: ++49 641 507 405, e-mail: labtalk@mt.com | | |
|---|---|---|
| DSC-Workshop | March 29.–30. 2022 | Giessen |
| TGA-Workshop | April 5.–6. 2022 | Giessen |
| DSC-Workshop | September 20.–21. 2022 | Giessen |

**France**
Cours et séminaires d'Analyse Thermique

| Renseignements et inscriptions par Paul Maillard, Mettler-Toledo S.A., 18-20 Av. de la pépinière, 78222 Viroflay Cedex, Tél: +33 1 30 97 16 54, e-mail: FormationClients@mt.com | | |
|---|---|---|
| Analyse Thermo Dynamique – DMA | 5 Décembre 2022 | 78222 Viroflay Cedex, France |
| Analyse Thermo Gravimétrique – TGA | 6 Décembre 2022 | 78222 Viroflay Cedex, France |
| Logiciel STAR® | 7 Décembre 2022 | 78222 Viroflay Cedex, France |
| Calorimétrie différentielle à balayage – DSC | 8 Décembre 2022 | 78222 Viroflay Cedex, France |
| Calorimétrie différentielle à balayage avancé – DSC Perfectionnement | 9 Décembre 2022 | 78222 Viroflay Cedex, France |

## Local TA Customer Courses

**Italia**
Corsi e Seminari di Analisi Termica

| Per ulteriori informazioni Vi preghiamo di contattare: Ottavio Lugaresi, Mettler-Toledo S.p.A., Novate Milanese, Tel: ++39 02 33 332 204, Fax: ++39 02 356 2973 e-mail: ottavio.lugaresi@mt.com | | |
|---|---|---|
| Corsi per Clienti: DSC base | A richiesta, date da definire | Milano |
| Corsi per Clienti: DSC avanzato | A richiesta, date da definire | Milano |
| Corsi per Clienti: TGA | A richiesta, date da definire | Milano |
| Corsi per Clienti: TMA | A richiesta, date da definire | Milano |
| Corsi per Clienti: DMA | A richiesta, date da definire | Milano |

**España**
Cursos y Semianros

| Para detalles de los cursos y seminarios, por favor contacte con: Francesc Català, Mettler-Toledo S.A.E., Tel: ++34 93 223 76 00, e-mail: francesc.catala@mt.com | | |
|---|---|---|
| Aplicaciones de las técnicas DSC y TGA en Polímeros | 19/04/2022 16:00 – 17:30 | On-line |
| Aplicaciones de las técnicas DSC y TGA en Farma | 11/05/2022 10:00 – 11:30 | On-line |
| Aplicaciones de las técnicas TMA y DMA en Polímeros | 16/06/2022 16:00 – 17:30 | On-line |
| Aplicaciones de las técnicas DSC y TGA en Polímeros | 20/09/2022 10:00 – 11:30 | On-line |
| Aplicaciones de las técnicas DSC y TGA en Farma | 27/10/2022 16:00 – 17:30 | On-line |

**India**
TA Customer Courses and Seminars

| For details of training courses and seminars, please contact: Pradeep Palshikar, Mettler-Toledo India Private Limited, Amar Hill, Saki Vihar Road, Powai, Mumbai 400 072 Tel: +91-22-28031 111 / 42910380 / 28031 380, Fax: +91-22-2857 5071, e-mail: pradeep.palshikar@mt.com | | |
|---|---|---|
| Innovative Applications of Thermal Analyzers to Pharmaceutical Industry (Pharma) | January 2022 | Not specified |
| Selecting the Right Crucibles for DSC and TGA Analysis (All) | February 2022 | Not specified |
| Thermal Analysis: Exclusive Solutions for Polymer Characterization (Polymer and Plastics, MPE) | March 2022 | Not specified |
| Thermal Analysis of Battery Components (Chemical, MPE, Battery) | April 2022 | Not specified |
| Thermal Analysis – Tips and Hints (All) | May 2022 | Not specified |

**Malaysia**
TA Customer Courses and Seminars

| For details of training courses and seminars, please contact: Joey Chee, Mettler-Toledo (M) Sdn. Bhd, Unit 1-01, Lot 8, Jalan Astaka U8/84, Seksyen U8, Bukit Jelutong, Shah Alam 40150 Selangor, Malaysia, Tel: (+603)-78445888, Fax: (+603)-78458773, e-mail: mtmymarketing@mt.com | | |
|---|---|---|
| DSC Analysis – Fundamentals and Applications | February 24, 2022 | Live broadcast |
| Thermal Analysis of Oil and Fats | April 14, 2022 | Live broadcast |
| TMA and DMA Analysis Techniques for Composites and Rubber | June 16, 2022 | Live broadcast |
| TGA Analysis – Fundamentals and Applications | August 18, 2022 | Live broadcast |

**Thailand**
TA Customer Courses and Seminars

| For details of training courses and seminars, please contact: Saowanij Kulthiwalert, Mettler-Toledo (Thailand) Limited, Tel: +66-2-7230338, Fax: +66-2-7196479 e-mail: saowanij.kulthiwalert@mt.com | | |
|---|---|---|
| 1. How to Choose the Right Crucible | April 2022 | Not specified |
| 2. The Characterization of Polymorphs by Thermal Analysis using DSC | May 2022 | Not specified |
| 3. Quality Assurance in the Production of Printed Circuit Boards | May 2022 | Not specified |
| 4. Thermal Analysis of Lithium-Ion Batteries | June 2022 | Not specified |

**Korea**
TA Customer Courses and Seminars

| For details of training courses, workshop and seminars, please contact: Dongmin Choi at Mettler-Toledo Korea, Tel: ++82 2 3498 3500 e-mail: Dongmin.Choi@mt.com, website: www.mt.com | | |
|---|---|---|
| TGA Application 세미나 | 2022 년 1 월 | 온라인 |
| 열분석 스쿨 | 2022 년 4 월 | 온라인 |
| DSC Application 세미나 | 2022 년 7 월 | 온라인 |
| 열분석 스쿨 | 2022 년 10 월 | 온라인 |

**North America**
TA Customer Courses and Seminars

| For details of training courses and seminars, please contact: Danielle Kimmel, Market Specialist, Materials Characterization METTLER TOLEDO, 1900 Polaris Parkway, Columbus, Ohio 43240, USA, Tel: 614-896-1728, e-mail: Danielle.Kimmel@mt.com | | |
|---|---|---|
| Solutions for Battery Characterization, Production, and Testing | January 13, 2022 | Broadcast |
| Thermogravimetric Analysis | January 27, 2022 | Broadcast |
| Moisture Content and Impact on Material Properties | February 17, 2022 | Broadcast |
| Determination of the Glass Transition | February 24, 2022 | Broadcast |
| Kinetics in Thermal Analysis | March 24, 2022 | Broadcast |
| Thermal Analysis of Thermoplastics | April 21, 2022 | Broadcast |
| Thermal Analysis of Thermoplastics | April 28, 2022 | Broadcast |
| Dynamic Mechanical Analysis | May 19, 2022 | Broadcast |
| Thermal Analysis of Textile Materials | June 23, 2022 | Broadcast |
| Thermal Analysis of Tires | July 28, 2022 | Broadcast |
| Safety Studies Using Thermal Analysis | August 25, 2022 | Broadcast |
| Thermal Analysis of Nanomaterials | September 29, 2022 | Broadcast |
| Validation in Thermal Analysis | October 27, 2022 | Broadcast |
| TOPEM | November 17, 2022 | Broadcast |
| Thermal Analysis of Elastomers | December 8, 2022 | Broadcast |

**Mexico**
TA Customer Courses and Seminars

| For details of training courses and seminars, please contact: Omar Hernandez Arguello, Technical and Application Consultant MatChar METTLER TOLEDO, Av. Ejército Nacional 340, Col. Polanco V Sección 11560 CDMX, Tel: +52 55 4840 9123, e-mail: Omar.Hernandez@mt.com, Visit: www.mt.com | | |
|---|---|---|
| Aplicaciones de las técnicas DSC y TGA en Polímeros | 19/04/2022 16:00 – 17:30 | On-line |
| Aplicaciones de las técnicas DSC y TGA en Farma | 11/05/2022 10:00 – 11:30 | On-line |
| Aplicaciones de las técnicas TMA y DMA en Polímeros | 16/06/2022 16:00 – 17:30 | On-line |
| Aplicaciones de las técnicas DSC y TGA en Polímeros | 20/09/2022 10:00 – 11:30 | On-line |
| Aplicaciones de las técnicas DSC y TGA en Farma | 27/10/2022 16:00 – 17:30 | On-line |

**China**
TA Customer Courses and Seminars

| For details of training courses and seminars, please contact: Nicole Dong at Mettler-Toledo Instruments (Shanghai) Co. Ltd. Tel: ++86 21 6485 0435, Fax: ++86 21 6485 3351, e-mail: Yanjia.huang@mt.com | | |
|---|---|---|
| Fundamental Courses (基础用户培训) | 2022/01/18 – 2022/01/21 | Shanghai+ Webcast |
| Fundamental Courses (基础用户培训) | 2022/03/22 – 2022/03/25 | Beijing+ Webcast |
| Advanced Courses (高级培训) | 2022/04/21 – 2022/04/22 | Guangzhou |
| Fundamental Courses (基础用户培训) | 2022/05/24 – 2022/05/27 | Guangzhou+ Webcast |
| Fundamental Courses (基础用户培训) | 2022/06/28 – 2022/06/29 | Shenyang+ Webcast |
| Fundamental Courses (基础用户培训) | 2022/08/30 – 2022/08/31 | Xian+ Webcast |
| Fundamental Courses (基础用户培训) | 2022/10/27 – 2022/10/28 | Changsha+ Webcast |
| Advanced Courses (高级培训) | 2022/11/22 – 2022/11/23 | Guangzhou |
| Fundamental Courses (基础用户培训) | 2022/12/18 – 2022/12/21 | Shanghai+ Webcast |
| TA Webinar (在线研讨会) | 2022/01/25 | Promote TA-News |
| TA Webinar (在线研讨会) | 2022/03/16 | Composites Webcast |
| TA Webinar (在线研讨会) | 2022/04/19 | Pharma Webcast |
| TA Webinar (在线研讨会) | 2022/05/04 | Polymer Webcast |
| TA Webinar (在线研讨会) | 2022/06/07 | Chemical safety |
| TA Webinar (在线研讨会) | 2022/07/07 | Crystallization application |
| TA Webinar (在线研讨会) | 2022/08/09 | Electronic Industry |
| TA Webinar (在线研讨会) | 2022/10/11 | Fiber application |
| TA Webinar (在线研讨会) | 2022/12/06 | Food application |
| TA Infodays (线下技术交流会) | 2022/01/12 | Guangzhou |
| TA Infodays (线下技术交流会) | 2022/03/15 | Nanjing |
| TA Infodays (线下技术交流会) | 2022/04/12 | Ningbo |
| TA Infodays (线下技术交流会) | 2022/05/10 | Qingdao |
| TA Infodays (线下技术交流会) | 2022/06/09 | Shenyang |
| TA Infodays (线下技术交流会) | 2022/08/10 | Lanzhou |
| TA Infodays (线下技术交流会) | 2022/10/14 | Changsha |
| TA Infodays (线下技术交流会) | 2022/12/14 | Shanghai |
| 2022 METTLER TOLEDO Flash DSC Forum (2022年梅特勒-托利多Flash DSC 技术交流峰会) | 2022/03/15 | Shanghai |

**Local TA Customer Courses:**

**UK:** Call: 0116 235 7070, e-mail: enquire.mtuk@mt.com
**Schweiz und Österreich:** Frau Janine Schindler, Tel: +49 641 507 405, e-mail: labtalk@mt.com
**Netherlands:** Bart Baggen, Tel: ++31 344 63 83 63, e-mail: bart.baggen@mt.com
**Belgium:** Philippe Larbanois, Tel: ++32 2 334 02 11, e-mail: philippe.larbanois@mt.com
**Slovenia:** Keith Racman, Tel: +386 1 547 4900, e-mail: keith.racman@mt.com
**Türkiye:** İstanbul, Tel: +90 216 400 20 20, e-mail: onur.cebeci@mt.com, nurdan.tarakci@mt.com
**České republice a Slovensku:** Michaela Veberová, Tel: +420 226 808 153, e-mail: michaela.veberova@mt.com
**Polska:** Piotr Witukiewicz lub Grazyna Czaplicka, Tel: +48 22 440 67 00
**Россия:** Егор Филатов, тел.: +7 495 777 07 77вн. 81-83, e-mail: egor.filatov@mt.com
**Sweden, Norway and Denmark:** Sebastian Östlund, Tel: +46 7245 392 32, e-mail: sebastian.ostlund@mt.com
**Finland:** Oy G. W. Berg & Co Ab, Tel: +358 201 255 255, e-mail: gwb@gwb.fi
**Brasil:** Tel: +55 11 4166-7400 Departamento de Marketing
**Latin America:** Francesc Català, Tel: ++34-932 237 615 (Spain), e-mail: francesc.catala@mt.com
**Singapore:** Dr. Fayaz, Contact no: +65 68900011
**Japan:** ラボインスツルメンツ事業部, Tel: 03-5815-5515, e-mail: marcom.jp@mt.com
**Taiwan:** Karen Chen at Mettler-Toledo Taiwan, Tel: +886-2-26578898 p102, e-mail: karen.chen@mt.com
**Australia and New Zealand:** Kai Robinson, Tel: +61 455 068 037, e-mail: kai.robinson@mt.com

For further information regarding meetings, products or applications, please contact your local METTLER TOLEDO representative and visit our website **www.mt.com**

## Editorial Team


Dr. A. Hammer
Chemist


Dr. D. P. May
Chemist


Dr. R. Riesen
Chem. Engineer


Dr. J. Schawe
Physicist


Dr. V. Chaudhary
Polymer Engineer


Dr. S. Domann
Journ. and Chem.


S. Dandekar
Physical Chemist


Dr. T. Oberholzer
Biochemist


Dr. G. Raihani
Biologist


U. Jörimann
Electr. Engineer


N. Fedelich
Chem. Engineer


Dr. E. Hempel
Physicist


Dr. M. Wagner
Chemist


Dr. M. Schubnell
Physicist


Dr. A. Bach
Chemist


Dr. S. Kakade
Chemist


N. Jing
Chemist


Dr. T. Dennenwaldt
Chemist


Dr. M. Reber
Chemist


Dr. J. Chee
Chemist

**METTLER TOLEDO Group**
Analytical Instruments
Local contact: www.mt.com/contacts

**www.mt.com/ta**
For more information